Environmental controls on CH4 emission from polygonal tundra on the micro-site scale in the Lena River Delta, Siberia

Torsten Sachs, Michael Giebels, Julia Boike, Lars Kutzbach

Environmental controls on CH4 emission from polygonal tundra on the micro-site scale in the Lena River Delta, Siberia

Journal:	*Global Change Biology*
Manuscript ID:	GCB-09-0727.R1
Wiley - Manuscript type:	Primary Research Articles
Date Submitted by the Author:	08-Feb-2010
Complete List of Authors:	Sachs, Torsten; Alfred Wegener Institute for Polar and Marine Research, Research Unit Potsdam Giebels, Michael; Technical University Braunschweig, Institute of Geoecology; Leibniz-Centre for Agricultural Landscape Research, Institute for Landscape Matter Dynamics Boike, Julia; Alfred Wegener Institute for Polar and Marine Research, Research Unit Potsdam Kutzbach, Lars; Ernst Moritz Arndt University of Greifswald, Institute of Botany and Landscape Ecology; University of Hamburg, Institute of Soil Science
Keywords:	Arctic, tundra, methane, permafrost, scaling, closed chambers, eddy covariance, Siberia
Abstract:	The carbon budgets of the atmosphere and terrestrial ecosystems are closely coupled by vertical gas exchange fluxes. Uncertainties remain with respect to high latitude ecosystems and the processes driving their temporally and spatially highly variable methane exchange. Problems associated with scaling plot measurements to larger areas in heterogeneous environments are addressed based on intensive field studies on two nested spatial scales in Northern Siberia. Methane fluxes on the micro-site scale (0.1–100 m2) were measured in the Lena River Delta from July through September 2006 by closed chambers and were compared to simultaneous ecosystem scale (104 m2–106 m2) flux measurements by the eddy covariance method. Closed chamber measurements were conducted almost daily on 15 plots in four differently developed polygon centers and on a polygon rim. Controls on methane emission were identified by stepwise multiple regression. In contrast to relatively low ecosystem-scale fluxes controlled mainly by near-surface turbulence, fluxes on the micro-site scale were almost an order of magnitude higher at the wet polygon centers and near zero at the drier polygon rim and high-center polygon. Micro-site scale

methane fluxes varied strongly even within the same micro-sites. The only statistically significant control on chamber-based fluxes was surface temperature calculated using the Stefan-Boltzmann equation in the wet polygon centers, while no significant control was found for the low emissions from the dry sites. The comparison with the eddy covariance measurements reveals differences in controls and the seasonal dynamics between the two measurement scales, which may have consequences for scaling and process-based models. Despite those differences, closed-chamber measurements from within the eddy covariance footprint could be scaled by an area-weighting approach of landcover classes based on high-resolution imagery to match the total ecosystem-scale emission. Our nested sampling design allowed for checking scaling results against measurements and to identify potentially missed sources or sinks.

Environmental controls on CH_4 emission from polygonal tundra on the micro-site scale in the Lena River Delta, Siberia

Torsten Sachs[1,#], Michael Giebels[2,*], Julia Boike[1], Lars Kutzbach[3]

[1]) Alfred Wegener Institute for Polar and Marine Research, Research Unit Potsdam, Telegrafenberg A43, 14473 Potsdam, Germany

[2]) Institute of Geoecology, Technical University Braunschweig, Langer Kamp 19c, 38106 Braunschweig, Germany

[3]) Institute of Botany and Landscape Ecology, Ernst Moritz Arndt University of Greifswald, Grimmer Str. 88, 17487 Greifswald, Germany

[#])now at: Helmholtz Centre Potsdam – GFZ German Research Centre for Geosciences, Telegrafenberg, 14473 Potsdam, Germany

[*]) now at: Leibniz-Centre for Agricultural Landscape Research, Institute for Landscape Matter Dynamics, Eberswalder Str. 84, 15374 Muencheberg, Germany

Corresponding author:

Torsten Sachs, Alfred Wegener Institute for Polar and Marine Research

Telegrafenberg A43, 14473 Potsdam, Germany

Phone: +49-331-288-2142

Fax: +49-331-288-2204

Email: torsten.sachs@awi.de

Keywords: Arctic, tundra, methane, permafrost, scaling, closed chambers, eddy covariance

Running title: Controls on tundra CH4 flux and scaling

Abstract

The carbon budgets of the atmosphere and terrestrial ecosystems are closely coupled by vertical exchange fluxes of carbon dioxide and methane. Uncertainties remain especially with respect to high latitude ecosystems and the processes driving their temporally and spatially highly variable exchange of methane with the atmosphere. To address the problems associated with scaling plot measurements to larger areas in such heterogeneous environments, we conducted intensive field studies on two nested spatial scales in Northern Siberian tundra. Methane fluxes on the micro-site scale (0.1–100 m^2) were measured in the Lena River Delta from July through September 2006 by closed chambers and were compared to simultaneous ecosystem scale (1 ha–1 km^2) methane flux measurements by the eddy covariance method at the same study site. Our study adds results from an area that is seriously underrepresented in current efforts to quantify carbon emissions from high latitude ecosystems. Closed chamber measurements of methane fluxes were conducted daily on 15 plots in four differently developed polygon centers and on a polygon rim. Controls on methane emission were identified by a stepwise multiple regression procedure. In contrast to the relatively low ecosystem-scale fluxes which were mainly controlled by near-surface turbulence and to a lesser extend by atmospheric pressure and soil temperature, fluxes on the micro-site scale were almost an order of magnitude higher at the wet polygon centers and near zero at the drier polygon rim and a high-center polygon. Micro-site scale methane fluxes varied strongly even within the same micro-sites. The only statistically significant control on chamber-based fluxes was surface temperature in the wet polygon centers, while no significant control was found for the low emissions from the dry sites. The comparison with the eddy covariance measurements reveals important differences in both the controls and the seasonal dynamics between the two measurement scales, which may have consequences for scaling and process-based models. However, despite those differences, closed-chamber

measurements from within the eddy covariance footprint could be scaled by an area-weighting approach of landcover classes based on high-resolution imagery to match the total ecosystem-scale emission remarkably well at the investigated polygonal tundra. Our nested sampling design allowed for checking scaling results against measurements and would have enabled us to identify potentially missed sources or sinks.

1. Introduction

In recent decades, methane (CH_4) has increasingly become a focus of studies investigating the carbon cycle and carbon budget as well as the feedback mechanisms increasing greenhouse gas emissions may have on the climate system. Despite these increased efforts, atmospheric concentration data and earth surface emissions still cannot be reconciled, and large uncertainties remain with regard to both mechanistic understanding of methane emissions and the distribution and strength of sources and sinks. Even new sources (Keppler *et al.* 2006; Walter *et al.* 2006) and mechanisms (Mastepanov *et al.* 2008; Sachs *et al.* 2008) are still being identified and discussed. While a general scarcity of data from the Arctic, especially from the extensive Russian tundra areas, is a major factor in this lack of understanding, it is exacerbated by the heterogeneity of the methane sink/source distribution as well as the large variability of methane emissions and the processes controlling these emissions, which vary over different spatial and temporal scales. This heterogeneity contributes to uncertainties in the global methane budget, especially by complicating any attempts at up-scaling emissions from point measurements to larger areas or even global estimates, as small-scale variability can substantially affect the statistics of large-scale variables (von Storch 2004).

Therefore, measurements of methane fluxes and their controls are required on multiple spatial and temporal scales in order to comprehensively understand methane dynamics (Bubier & Moore 1994). At key sites, each measurement should ideally be nested within the footprint of the next larger scale measurements to develop up-scaling methods in small, verifiable steps.

Closed-chamber techniques are widely used for small-scale measurements and allow for good spatial coverage (Whalen & Reeburgh 1990; Christensen *et al.* 1995; Reeburgh *et al.* 1998; Wickland *et al.* 2006). However, they represent an intrusive method and can affect the measured variable even if care is taken to avoid the many potential biases this method is prone to. In a nested approach, results can be checked against other methods such as the eddy covariance technique, thus helping to reduce uncertainties (Fan *et al.* 1992; Riutta *et al.* 2007; Fox *et al.* 2008; Kulmala *et al.* 2008).

We applied such a nested approach in our investigation of methane emissions from northern Siberian wet polygonal tundra in the Lena River Delta. An eddy covariance (EC) system capable of continuous high-resolution methane flux measurements was installed at the site in 2002 and has delivered valuable flux data on the ecosystem scale (Sachs *et al.* 2008; Wille *et al.* 2008). Existing closed chamber sites for studies of the effect of microrelief and vegetation on methane emission (Wagner *et al.* 2003; Kutzbach *et al.* 2004) were located 700 m south of the tower site in an area that was generally drier and more elevated. Thus, in 2005, fifteen closed chambers were installed at five different micro-sites within the eddy covariance footprint and operated simultaneously to the EC system.

The objectives of this paper are to (1) investigate the spatial variability of methane fluxes from wet polygonal tundra within the eddy covariance footprint, (2) identify the dominant processes and controls governing small-scale methane dynamics, (3) compare the results to eddy covariance measurements in order to identify differences or similarities in the seasonal dynamics and the dominant processes and controls.

2. Study area

The study site was located on Samoylov Island near the Russian-German Research Station Samoylov Island, 120 km south of the Arctic Ocean in the southern central Lena River Delta (72°22'N, 126°30'E) (Fig. 1). Samoylov Island is located in the active delta landscape, which covers about 65% of the total 32,000 km² delta. During the past ten years, Samoylov Island has been the focus of a wide range of studies on surface-atmosphere gas and energy exchange, soil science, hydrobiology, microbiology, cryogenesis, and geomorphology (Schwamborn *et al.* 2002; Boike *et al.* 2003, 2008; Kutzbach *et al.* 2004, 2007; Abramova *et al.* 2007; Liebner & Wagner 2007; Sachs *et al.* 2008; Wille *et al.* 2008).

Samoylov Island covers an area of about 5 km². The western part of the island (2 km²) is a modern floodplain with elevations from 1 to 5 meters above sea level (a.s.l.), which is flooded annually during river break-up. The study site is located in the center of the eastern part of the island (3 km²) with elevations from 10 to 16 meters a.s.l. which is composed of sediments of a Late-Holocene river terrace (Fig. 2). The surface of the terrace is characterized by wet polygonal tundra with a flat mesorelief and a pronounced regular micro-relief caused by the development of low-center ice wedge polygons. The typical elevation difference between depressed polygon centers and elevated polygon rims is up to 0.5 m (Kutzbach 2006). The poorly drained and hence mostly inundated centers are characterized by *Typic Historthels*, while *Glacic* or *Typic Aquiturbels* dominate at the dryer but still moist polygon rims (Soil Survey Staff 1998; Kutzbach *et al.* 2004). As the summer progresses, these soils typically thaw to a depth of 30 cm to 50 cm. Hydrophytic sedges as well as mosses dominate the vegetation in the wet polygon centers (Kutzbach *et al.* 2004). Polygon rims are dominated by mesophytic dwarf shrubs, forbs, and mosses. Surface classification of aerial photographs shows that elevated and dryer areas cover approximately 62% of the tundra surrounding the study site, while depressed and wet polygon centers and troughs cover only about 10%. Open and overgrown water makes up 28% of the area (Schneider *et al.* 2009).

The climate in the region is arctic continental climate characterized by very low temperatures and low precipitation. Mean annual air temperature at the meteorological station on Samoylov Island was –14.7°C and mean liquid precipitation was 137 mm, ranging from 72 mm to 208 mm in a period from 1999 to 2005 (Boike *et al.* 2008). Meteorological conditions can change rapidly throughout the growing season depending on the prevailing synoptic weather conditions, which cause either advection of cold and moist air from the Arctic Ocean or warm and dry air from continental Siberia, respectively. The region experiences polar day from 7 May to 8 August and polar night from 15 November to 28 January. Snowmelt and river break-up typically start in the first half of June, and the growing season lasts from mid-June through mid-September. The continuous permafrost in the delta reaches depths of 500 to 600 meters (Grigoriev 1960) and is characterized by very low temperatures with the top-of-permafrost temperature on Samoylov being approximately –10°C (Boike *et al.* 2003).

3. Investigation sites

Five different micro-sites (four polygons and a rim) characteristic of the prevalent surface and vegetation features in the eddy covariance fetch were established within 40 m of the EC tower and equipped with boardwalks, wells for water level measurements, and three chamber collars each (Fig. 2).

Polygon 1 was a low-center polygon with standing water in the center. The northern side of the polygon rim showed signs of beginning degradation, which might serve as a hydraulic connection to surrounding polygon troughs. Polygon 2 was a high-center polygon with no standing water in the center due to drainage into surrounding thermokarst cracks and troughs. Polygon 3 was a low-center polygon with a massive rim on the western side and a completely degraded rim on the eastern side, where a large thermokarst crack of more than 2 m depth was located. There was standing water in the polygon center throughout most of the growing season. Polygon 4 was a low-center polygon with no apparent rim degradation and no apparent hydraulic connection to surrounding cracks or troughs. It usually maintained the highest water level of all investigated polygon centers. The polygon rim micro-site was underlain by a massive ice wedge and draining into polygon 3 to the east and the crack.

A detailed vegetation cover is given in Table 1 (data provided by M. Minke, 2006). While many species are typical for a rich fen, the polygonal tundra is not a classical fen. Ultimately, all water in polygon centers is provided by rain or snow. However, some of that water also drains into polygon centers from surrounding rims. Nutrient input may be from dust storms and otherwise from fluvial sediments through upward migration into polygon rims due to cryoturbation. Base saturation and pH are relatively high, however, in comparison to active flood plains, the polygonal tundra terrace is rather nutrient limited. A schematic overview and exemplary photographs of the dominant micro-site types are given in Figure 3. The organic layer is about 5 cm thick on polygon rims and about 30 cm in polygon centers.

The root density is high within the top 15 cm of the soil and then decreases towards deeper horizons. At our site, the active layer is deeper in low-center polygons (up to 40 cm) than on polygon rims and high-center polygons (about 20 cm). At the climate station 700 m south of the closed chamber sites, this relationship is reversed with a deeper active layer at the top of the polygon rims than in the centers. Generally, a measurable water table is only present in low-center polygons, but high-center polygons and rims remain very moist at least right above the permafrost table as indicated in the figure. Temperature gradients are generally steeper in rims and high-center polygons, which also reach higher surface temperatures than water-inundated low-center polygons. The CH_4 concentration in the noninundated soil is close to ambient in the aerobic soil horizons and increases strongly just above the permafrost table, where anaerobic conditions dominate (S. Liebner, personal communication).

4. Methods

4.1. Closed chamber set-up and measurements

Three 50 cm x 50 cm PVC chamber collars with a water-filled channel as a seal were installed in each of the four polygon centers and along the rim and inserted 10-15 cm into the active layer. Chambers were made of opaque PVC and clear PVC, respectively, for light and dark measurements. Chamber volume was 12.5 l at the high-center and rim micro-sites and 37.5 l at the other sites where higher vegetation did not allow for the use of small chambers.

Manual chamber measurements at all 15 plots were made daily from 13 July through 19 September 2006 with both clear and opaque chambers, resulting in 6 measurements per day and micro-site. Sample air was drawn from a port on top of the chamber every 45 s for eight to ten minutes for simultaneous analysis of CO_2, CH_4, and water vapor using a photo-acoustic infrared gas spectrometer Innova 1412 with optical filters UA0982 for CO_2, UA0969 for CH_4, and SB0527 for water vapor (INNOVA AirTech Instruments, Denmark). A membrane pump was connected to two other ports and circulated chamber headspace air through perforated dispersive tubes for mixing.

Because of water interference with the CH_4 optical filter, sample air was dried prior to entering the analyzer using 0.3 nm molecular sieve (beads, with moisture indicator; Merck KGaA, Darmstadt, Germany). Temperature and pressure inside the chamber were logged continuously by a MinidanTemp 0.1° temperature logger (Esys GmbH, Berlin, Germany) and the Innova 1412, respectively.

Additional variables measured at the eddy covariance system and an automated long-term monitoring station 700 m south of the EC tower include air temperature, relative humidity, incoming and outgoing solar and infrared radiation, photosynthetically active radiation (PAR), barometric pressure, precipitation, and soil temperature at various depths.

Manual measurements at each micro-site during chamber deployment included thaw depth using a steel probe, soil temperatures in 5 cm depth intervals, and water level.

4.2. Non-linear flux calculation

The most widely used method for calculating fluxes from the change of concentration in the chamber headspace over time is by linear regression under the assumption that by keeping chamber closure time short, the concentration change is approximately linear. However, (Kutzbach *et al.* 2007) showed that linear regression is frequently not appropriate based on four sets of closed chamber CO_2 data, including those gathered during the measurement campaign reported on here. We found the conclusions for the CO_2 data to also hold for CH_4 (e.g. in Fig. 4) and therefore used the non-linear exponential regression model proposed by Kutzbach *et al.* (2007) to describe CH_4 evolution over time in the chamber headspace:

$$c(t) = f_{\exp}(t) + \varepsilon(t) = \beta_1 + \beta_2 \exp(\beta_3 t) + \varepsilon(t) \qquad (1)$$

where $\varepsilon(t)$ is the residual error at measurement time t.

At the beginning of the measurement, gas fluxes are assumed to be least disturbed by chamber deployment, and thus, the initial slope of the regression curve $f_{\exp}'(t_0) = (\beta_2 \beta_3)$ is used for flux calculation:

$$F_{CH4}(t_0) = \frac{dc}{dt}(t_0)\frac{pV}{RTA} = f'_{\exp}(t_0)\frac{pV}{RTA} = \beta_2 \beta_3 \frac{pV}{RTA} \qquad (2)$$

where p is air pressure, R is the ideal gas constant, T is the temperature (in Kelvin) and V and A are the volume and basal area of the chamber.

Calculated fluxes were thoroughly screened and all fluxes with a residual standard deviation greater than 0.3 ppm were excluded from further analysis.

4.3. Model development

Measurements were summarized by averaging the six individual measurements at each micro-site and day. In order to identify statistically significant explanatory variables for the measured methane fluxes, we used multiple linear regressions, starting with a descriptive regression model including all available variables:

$$F_{CH4} = c_0 + c_1 \cdot x_1 + c_2 \cdot x_2 + \ldots + c_n \cdot x_n \qquad (3)$$

We then eliminated all non-significant variables in a stepwise procedure:

First, data were tested for multi-collinearity following Schuchard-Ficher *et al.* (1982). If multi-collinearity was present, variables were dropped until all remaining variables were approximately orthogonal. Next, the residuals of the reduced model were tested for autocorrelation using the Durbin-Watson test (or d-test).

If no autocorrelation was found, the multiple regression coefficient of determination R^2 was tested for significance using the *F*-test:

$$F(df_1 = q, df_2 = n - q - 1) = \frac{R^2 \cdot (n - q - 1)}{q \cdot (1 - R^2)} \qquad (4)$$

where *df* indicates degrees of freedom, n is the number of data points and q is the number of predictor variables.

If R^2 was significant, the correlation coefficients c ($i = 1,2,\ldots,n$) were tested for significance using the *t*-test. The reduced model that passes these tests provides predictors of the methane flux with a statistically significant explanatory power, i.e. it identifies not necessarily the best fit to the data but the significant and most likely process drivers.

245 After the parameter selection process, the resulting regression model was fitted to the means of the six replicate measurements per day and micro-site using the inverse square of the mean standard error of these six measurements as a weight, such that points with large errors were given less weight in the fitting process. Cumulative CH_4 fluxes over the measurement period were calculated by integrating the modeled hourly flux time series. The uncertainty of the cumulative fluxes was assessed by error propagation using the RMSE of the regression models as uncertainty indicator for the hourly modeled flux values.

5. Results

5.1. Meteorology

At the beginning of the measurement period, air temperatures had just dropped from a daytime summer record of up to 28.9°C on 11 July (mean 18.3°C, minimum 8.9°C) to well below 10°C (Fig. 5). Fluctuations between daytime and nighttime temperatures were strong throughout July with mean temperatures rising from 8.4°C in the first week of measurements to 12.2°C in the third week. The maximum daily mean temperature during the measurements period was reached on 31 July at 18.5°C. A storm system with heavy precipitation of up to 23 mm per day and prolonged periods of mean hourly wind speeds around 10 m s^{-1} caused daily mean temperatures to drop sharply to as low as 4.2°C in the first week of August. Mean daily temperatures never exceeded 11.9°C for the remaining season and remained between 2.3°C and 11.9°C during August. Another storm system in the first week of September yielded 34 mm of precipitation within three days and wind speeds exceeding 20 m s^{-1}. Temperatures continued to decrease and reached a daily minimum at –5.2°C on 9 September. Mean daily temperature was well below zero for the entire week from 8 September to 15 September and caused the mean September temperature (1 September – 19 September) to be below freezing despite increasing temperatures during the last week of the measurement period. The second week of September was characterized by extremely low atmospheric pressure (down to 98 kPa) and frequent snow storms with wind speeds above 10 m s^{-1}. Snow started to accumulate on 12 September and reached depths of 8–10 cm in polygon centers and 2–6 cm on elevated areas, but all snow had disappeared on 18 September after advection of warmer air from the south. By mid-September, all water bodies except for the large thermokarst lakes were covered with ice up to 8 cm thick and soils were frozen up to approximately 10 cm depth. Long-term temperature data are available from Tiksi, which is located 110 km south-east of Samoylov Island but characterized by very similar temperatures. Temperature conditions in

2006 were within ±1°C of the long-term average in July (7°C), August (7°C), and September (1°C). The average daily wind speed was 5.3 ms^{-1} during the study period, which is 0.6 ms^{-1} higher than in 2003 and 2004 (Kutzbach 2006). Winds from east southeast were clearly predominant, but west-northwesterly and southern winds also occurred frequently (data not shown).

5.2. Methane fluxes and controls

Fluxes were averaged across six measurements per micro-site and day (two measurements on each of three plots per micro-site) and are reported with the standard deviation as a measure of within-site spatial variability and the averaged standard error of the measurements (Fig. 6). In general, methane emission was similar among the wet and inundated low-center polygons and differed from fluxes at the high-center and rim micro-sites by an order of magnitude. At the low-center polygons, the monthly averaged emissions decreased by about 30% from July to August and by about 70% from August to September.

At the wet and low-centered Polygon 1 (Fig. 6a), the average methane flux during the measurement period was 77.88 mg m^{-2} d^{-1} decreasing from a July average of 121.16 mg m^{-2} d^{-1} to 83.81 mg m^{-2} d^{-1} in August and 27.69 mg m^{-2} d^{-1} in September. The maximum methane flux occurred on 24 July at 278.40 ± 307.18 mg m^{-2} d^{-1} (standard error: 39.34 mg m^{-2} d^{-1}), when surface temperatures exceeded 22°C and a day after air temperatures exceeded 20°C. The minimum flux was recorded on 12 September at 9.33 ± 15.77 mg m^{-2} d^{-1} (standard error: 14.08 mg m^{-2} d^{-1}) during the frost period. The water level in this polygon never dropped below the surface during the entire measurement period and ranged from 0 to 9.5 cm above the surface. Peak water levels were reached after precipitation events at the beginning of August and the beginning of September as well as after snow melt and thawing at the end of the campaign. The active layer depth gradually increased from 18 cm at the beginning of the measurement period to a maximum of 35 cm, which was reached on 4 September. During the frost period a refreezing from the bottom decreased the active layer depth to 32 cm by 19 September.

At the relatively “dry” and high-centered Polygon 2 (Fig. 6b), the average methane flux during the measurements period was significantly lower at 10.49 mg m^{-2} d^{-1} with no clear seasonal trend from a July average of 9.43 mg m^{-2} d^{-1} to 11.28 mg m^{-2} d^{-1} in August and 10.05 mg m^{-2} d^{-1} in September. The maximum methane flux occurred on 11 September at 39.07 ± 55.28 mg m^{-2} d^{-1} (standard error: 38.75 mg m^{-2} d^{-1}), and the minimum flux was recorded on 12 September at -1.87 ± 4.13 mg m^{-2} d^{-1} (standard error: 5.12 mg m^{-2} d^{-1}). The water level in this polygon remained slightly above the permafrost table and never reached the surface during the entire measurement period. It ranged from 16 cm to 4.5 cm below the surface and peak water levels were reached after the precipitation event at the beginning of August and after thawing towards the end of the campaign. The active layer depth increased less than in the low-center polygons from 14 cm to 21 cm. No clear refreezing from the bottom was observed.

The wet and low-centered Polygon 3 (Fig. 6c) showed the largest methane emissions. The average methane flux during the measurements period was 99.98 mg m^{-2} d^{-1} decreasing from a July average of 150.93 mg m^{-2} d^{-1} to 110.58 mg m^{-2} d^{-1} in August and 28.91 mg m^{-2} d^{-1} in September. The maximum methane flux occurred on 1 August at 363.82 ± 259.81 mg m^{-2} d^{-1} (standard error: 42.39 mg m^{-2} d^{-1}) when daytime temperature exceeded 20°C and a day after daytime temperatures had reached 26°C. The minimum flux was recorded on 15 September at 8.81 ± 7.29 mg m^{-2} d^{-1} (standard error: 7.29 mg m^{-2} d^{-1}) during the frost period. Except on the first two days of measurements, the water level in this polygon never dropped below the surface and ranged from 0 to 8.5 cm above the surface. Peak water levels were reached after precipitation events at the beginning of August and the beginning of September as well as after snow melt and thawing at the end of the campaign. The active layer depth gradually increased from 19 cm at the beginning of the measurement period to a maximum of

37 cm, which was reached on 4 September. During the frost period a refreezing from the bottom decreased the active layer depth to 33 cm by 19 September.

At the inundated and low-centered Polygon 4 (Fig. 6d), the average methane flux during the measurements period was 80.75 mg m^{-2} d^{-1} decreasing from a July average of 123.21 mg m^{-2} d^{-1} to 87.76 mg m^{-2} d^{-1} in August and 23.49 mg m^{-2} d^{-1} in September. The spatial variability in this polygon was much lower than in Polygon 1 and 3, as were the peak fluxes. The maximum methane flux occurred on 26 July at 161.58 ± 118.10 mg m^{-2} d^{-1} (standard error: 29.91 mg m^{-2} d^{-1}) when surface temperatures exceeded 21°C. The minimum flux was recorded on 15 September at 1.78 ± 3.34 mg m^{-2} d^{-1} (standard error: 5.03 mg m^{-2} d^{-1}) during the frost period. This polygon had the highest water level after precipitation events (up to 12.5 cm) and throughout July but also showed a more pronounced drying in August, causing the water level to drop slightly below the surface at the end of August. In September, the water level resembled that of Polygon 1. The active layer depth gradually increased from 24 cm at the beginning of the measurement period to a maximum of 40 cm, which was reached on 4 September. During the frost period a refreezing from the bottom decreased the active layer depth to 36 cm by 19 September.

At the elevated and well-drained polygon rim (Fig. 6e), the average methane flux during the measurements period was the lowest of all sites at 4.94 mg m^{-2} d^{-1}, increasing from a July average of 2.14 mg m^{-2} d^{-1} to 4.07 mg m^{-2} d^{-1} in August and 9.15 mg m^{-2} d^{-1} in September. The maximum methane flux occurred on 11 September at 28.22 ± 36.86 mg m^{-2} d^{-1} (standard error: 18.60 mg m^{-2} d^{-1}) and the minimum flux was recorded on 8 September at –3.57 ± 20.31 mg m^{-2} d^{-1} (standard error: 10.14 mg m^{-2} d^{-1}) when temperatures dropped below freezing. Typically, the standard error of the measurements was around ± 25 mg m^{-2} d^{-1} for Polygon 1, 3, and 4, and about ± 10 mg m^{-2} d^{-1} for the drier micro-sites. The spatial standard deviation was around ± 43 mg $m^{-2}d^{-1}$ in Polygon 1, 3, and 4, and about ± 10…15 mg m^{-2} d^{-1} at the drier sites. Polygon 4 showed less spatial variability than Polygon 1 and 3. Except on the polygon rim, spatial standard deviation decreased strongly towards the end of the season, most pronouncedly in the low-center polygons.

It was not possible to construct multidimensional regression models with independent and significant parameters. The predictor variable with the highest explanatory power within the final one-dimensional model for the low-center polygons was surface temperature (Table 2; Fig. 7). Except for the underestimation of the extreme flux peaks on 24 July and 1 August at Polygon 1 and Polygon 3, the modeled methane flux agreed well with measured fluxes (mean *RMSE* = 1.43 mg m^{-2} d^{-1}). The best fit (*RMSE* = 1.33 mg m^{-2} d^{-1}) was obtained at Polygon 4, which did not show any major outliers in the flux data.

At Polygon 2 (high-center) and at the polygon rim, very low methane concentrations in the closed chamber system frequently caused the analyzer to reach its detection limit, resulting in noisy data and a high exclusion rate during flux calculation. No statistically significant correlation with any of the observed environmental parameters was found.

Cumulative fluxes during the measurement period were similar at Polygon 1 and 4 with 3.95 ± 0.0020 g m^{-2} and 4.26 ± 0.0023 g m^{-2}, respectively. Polygon 3 emitted about 25% more methane than Polygon 1 amounting to a cumulative flux of 4.93 ± 0.0031 g m^{-2}. At the drier micro-sites, cumulative fluxes were 0.72 ± 0.078 g m^{-2} at the high-center site and 0.34 ± 0.047 g m^{-2} at the rim site.

6. Discussion

6.1. Environmental controls on micro-site methane emission

Very wet polygon center (micro-sites 1, 3, and 4)

The single parameter with the highest explanatory power for the observed CH_4 fluxes and statistical significance at the three low-center polygon sites was surface temperature. Many studies found relationships between soil temperature in different depths and methane flux (Whalen & Reeburgh 1988; Bubier 1995; Christensen *et al.* 1995; Bellisario *et al.* 1999; Nakano *et al.* 2000), but only few (Hargreaves *et al.* 2001) identified surface temperature as a predictor of methane flux or even measured it. This finding might be due to our strict exclusion criteria and the significantly dampened variability of soil temperatures at our site. A shallow active layer and cold permafrost reduce short-term variability already close below the surface, and thus the highly variable surface temperature is better suited to predict highly variable methane fluxes than soil temperature with little variability, at least on the daily timescale investigated here. Nevertheless, soil temperatures are closely correlated with surface temperature, and thus surface temperature can be seen as a master variable representing the entire soil thermal regime. Roulet *et al.* (1992) found significant temperature relationships for only 3 out of 24 sites (beaver ponds and swamp), but the slopes of their regression (5.5 mg m^{-2} d^{-1} °C^{-1}, 7.0 mg m^{-2} d^{-1} °C^{-1}, and 7.3 mg m^{-2} d^{-1} °C^{-1}) were similar to the slopes in our relationships (table 2).

Temperature directly influences microbial activity (Arrhenius 1909; Conrad 1989) and several studies found relationships between soil or peat temperature and methane flux (Whalen & Reeburgh 1988; Bubier 1995; Christensen *et al.* 1995; Bellisario *et al.* 1999; Nakano *et al.* 2000), while others did not find a relationship (Wagner *et al.* 2003; Wickland *et al.* 2006). In principal, a temperature change affects both methanogens and methanotrophs and thus, its net effect on methane flux could be expected to cancel out. However, microbial populations on Samoylov Island were found to be well adapted to their environment and in particular, methanotrophic bacteria are characterized by lower temperature optima (Liebner & Wagner 2007). With methanotrophs more sensitive to increased temperatures, the balance can be expected to shift towards more methane production at higher temperatures.

Kutzbach *et al.* (2007) found surface temperature and not soil temperature as the best predictor variable for ecosystem respiration at the same study site, which was explained by the importance of above-ground plant respiration. Vegetation might also explain the controlling influence of surface temperature in this study if surface temperature is seen as an indicator for plant productivity. Vegetation plays an important role in the methane cycle, supplying substrate for methanogens, in some cases (e.g. sedges) oxygen for methanotrophs, and a conduit for methane release to the atmosphere (Morrissey *et al.* 1993; Whiting & Chanton 1993; Bubier 1995; Schimel 1995; King *et al.* 1998, 2002; Bellisario *et al.* 1999; Joabsson & Christensen 2001). At our site, plant-mediated methane transport was found to account for 27…66% of overall methane fluxes (Kutzbach *et al.* 2004). We did not find significantly different emission rates between measurements with clear chambers and those with opaque chambers, suggesting that there was no stomatal effect in plant-mediated methane flux.

Another effect of increased temperatures is decreasing solubility of methane in the water inundating the low-center polygons, thus resulting in increased release of methane from the water column into the atmosphere. For example, at the typical thaw depth of 30 cm in a water-saturated polygon center, with an assumed porosity of 0.7, and a maximum CH_4 saturation of the water column, a temperature change of 1.5°C (over the entire depth) would lead to an additional loss of about 272 mg CH_4 m^{-2} d^{-1}.

While methane emission was found to increase with higher water levels in many studies (e.g. Suyker *et al.* 1996; Friborg *et al.* 2000; Wagner *et al.* 2003), there was no correlation between water level and methane emission at our site on the daily time scale. This may be due to the fact that in low-center polygons, where most of the methane was emitted, the water level remained at or above the soil surface at all times and thus fluctuations in water level did not change the ratio of oxic/anoxic soil column. In fact, the dampened methane emission dynamics at Polygon 4, which had the highest water level during the measurement period, suggests that water levels above the surface may actually hinder methane emission by submerging vegetation and presenting a barrier to both soil-diffusive flux and plant-mediated flux. Bellisario *et al.* (1999) also found an inverse relationship between water table and methane flux but did not discuss the finding further. Zona & Oechel (2008) also found that in certain conditions, a drop in water table caused increased methane flux in a large-scale manipulation experiment in Arctic tundra in Barrow, Alaska. However, on the seasonal time scale, the water table explains about 85 % of the spatial variability of methane fluxes at the investigated polygonal tundra ($R^2_{adj} = 0.85$; $n = 5$).

Polygon rims & high-center polygons (micro-sites 2 & 5)

Polygon rims and high-center polygons appear to behave similarly despite strongly differing soil conditions (i.e. cryoturbated mineral soils on the rims vs. organic layers and peat in the high-center). No significant predictor was found for the high-center and rim site flux data, which were often low enough to reach the detection limit of the analyzer. However, higher air temperatures could be expected to not affect the methanogenic communities as much as in low-center polygons since these are mostly closer to the permafrost table where temperatures are dampened. Higher temperatures might increase the diffusive flux of methane but at the same time, drying of pore space and an increasing fraction of air-filled pores decreases the anaerobic soil volume needed for methane production. In addition, the anaerobic zone of methane production is usually deeper than the root horizon, and thus the net effect of increased temperature at drier sites is either negligible or at most a slight decrease in emissions. Lower temperatures usually accompanying precipitation events, on the other hand, may inhibit methane oxidation in the upper soil layers, further shifting the balance towards methane production. This is supported by Whalen & Reeburgh (1996) who found the lowest methane oxidation rates in boreal soils during experiments combining high moisture contents and low temperatures. The most pronounced effect on methane emission from these sites is expected to be that of precipitation and temporarily rising water levels which shift the distribution of aerobic/anaerobic soil volume towards anaerobic conditions, favoring methane production. At the same time, water percolating into the pore space will displace methane left in those pores and increase the advective flux. The net effect is a transient increase in methane production and emission from these micro-sites during periods of heavy precipitation and transient rises in water levels.

Open water surfaces

Open water surfaces are an important feature of the polygonal tundra and include relatively small but deep thermokarst cracks as well as ponds and larger lakes. Only exploratory closed chamber measurements were conducted on open water surfaces in this study. At these micro-sites, higher temperatures can increase the diffusive flux of methane but will most likely not affect methane production in the sediments underneath deeper water columns, unless the water bodies are clear and shallow enough for the sun to reach and warm the bottom sediments.

Open water surfaces are mostly affected by increased wind speeds. Diffusive and turbulent gas transfer between water and atmosphere is known to be proportional to the third power of the wind speed (Wanninkhof & McGillis 1999). In addition, storm systems are associated with decreasing atmospheric pressure, which was observed to increased methane flux by ebullition (Spott 2003). These micro-sites must be included in future small-scale measurements within the eddy covariance footprint in order to accurately scale chamber flux measurements to larger areas. Spott (2003) measured methane fluxes from water bodies of the polygonal tundra on Samoylov Island by closed chambers and found open water surfaces to emit between 1.9…9.9 mg m^{-2} d^{-1} during calm conditions while vegetated areas emitted up to 88.65 mg m^{-2} d^{-1}.

6.2. Comparison of closed chamber vs. eddy covariance methane fluxes and their controls on different scales

Simultaneous eddy covariance measurements of methane flux at the same site are described in Sachs *et al.* (2008) and – in combination with the results reported here – constitute the first study of methane emission from a Siberian arctic tundra site on different but nested scales. The comparison of micro-site fluxes from closed chamber data and ecosystem-scale fluxes of the eddy covariance system (Sachs *et al.* 2008) reveals differences both in terms of the dominant controls on methane flux as well as the seasonal variation of the fluxes (Fig. 8). On the ecosystem scale, no clear seasonal course was visible, although maximum fluxes did occur during the first week of August. On the micro-site scale, however, low-center polygons showed a decrease of methane emission from July to August by about 30% and a pronounced decrease from August to September by 70%, which is more in line with most studies (e. g. Whalen & Reeburgh 1988; Christensen *et al.* 1998; Wagner *et al.* 2003). The drier micro-sites, on the other hand, did not show any seasonal course and thus appear more comparable to the seasonal dynamics on the ecosystem scale.

In addition to the differing seasonal dynamics, peak methane emissions on the different scales did not occur on the same dates. Ecosystems scale emission peaks were usually associated with high wind speed, low atmospheric pressure, and precipitation events, and the best predictor of ecosystem scale methane emission was near-surface turbulence. The very few identifiable peaks at the drier micro-sites also tend to coincide with these weather conditions, while emission peaks at low-center polygons typically occurred during warm and dry days. At the end of the season, methane fluxes on the different scales diverge completely, with ecosystem scale and drier micro-site fluxes increasing during the last week while low-center polygon emissions reached their minima during the frost period.

Surface classification and flux weighting

Surface classification of high resolution aerial images reveals a distribution of these micro-sites which is likely to be wrongly estimated by simple visual assessment in the field: the very wet high methane emission sites only constitute 24% of the area while relatively drier and moderately moist sites occupy 62% of the area (Schneider *et al.* 2009; S. Muster, personal communication). If water with emergent vegetation is classified separately from inundated low-center polygons where water levels are just at or slightly above the surface, the fraction of low-center polygons is reduced to about 10%, while overgrown water covers about 14% of the area (Schneider *et al.* 2009). Open water without vegetation is present in about 14% of the area (Schneider *et al.* 2009; S. Muster, personal communication). Table 3 provides typical methane emissions for each surface class and the fraction of the surface it covers during August. Ebullition fluxes according to Spott (2003) were 4.17 mg m^{-2} d^{-1} on average (measured at three water bodies) but may have been underestimated due to the applied closed chamber approach which reduces water turbulence. Adding ebullition flux to the emissions from open water surfaces can change the total flux but would have to be at least three times higher than the diffusive flux to change the total flux estimate by 5% or more. Assuming decreased emissions from very wet soils and increased emissions from drier soils during periods of lower temperatures and higher wind speeds can increase the total flux even without changing the emission rate from water bodies, which, however, will also increase due to the mechanism discussed above. This thought experiment demonstrates that on a landscape scale, the effects of weather-induced changes in methane emission can easily be the opposite of what is observed on a small scale or expected based on previous (mostly closed chamber) studies.

These discrepancies in the results on the different scales highlight the need for integrated investigations of methane dynamics on multiple nested scales, and in particular the need for more non-intrusive and spatially integrating measurements such as by eddy covariance or airborne instruments, allowing to compare extrapolated results from small scales to actual data on the next larger scale. At key sites, scaled emissions should be checked in small steps to increase confidence and reduce uncertainties in scaling procedures. In this study, closed-chamber measurements from within the eddy covariance footprint could be scaled by an area-weighting approach of landcover classes to match the total ecosystem-scale emission remarkably well despite the different controls and methane dynamics on the two scales. On the other hand, another up-scaling study by Schneider *et al.* (2009) reports total emissions from the same types and distribution of landcover classes that are about 34% lower than in this study. The closed chamber measurements forming the basis of the Schneider *et al.* (2009) upscaling were located 700 m south of the eddy covariance tower in a generally drier and more elevated area (Wagner *et al.* 2003). The classification used in their upscaling, however, was based on two aerial image scenes, both of which cover wetter areas in the center of the island. If a classification of the actual measurement site results in the same landcover classes, the discrepancy between the two studies implies that either differences in flux calculation from closed chamber data (linear regression in Schneider *et al.* (2009) vs. nonlinear regression here) or spatial heterogeneities cause the significant difference between these two estimates. If differences in the flux calculation caused the discrepancy, this underlines the importance of accurate flux determination as discussed in Kutzbach *et al.* (2007). If spatial heterogeneity is the reason, it demonstrates clearly that small-scale measurements of methane can not readily be applied to scales beyond the "next step" in the scaling ladder. And if the classification of the actual measurement site results in different landcover classes, it emphasizes the importance of obtaining data and information intended to be integrated under as similar conditions as possible.

Difficulties in upscaling emissions governed by highly local controls were already identified by Bubier & Moore (1994) and multiscale studies were recommended. Nonetheless, most studies extrapolate emissions from point measurements with little or no ability to validate results with measurements on the larger scale. Heikkinen *et al.* (2004) measured carbon and methane fluxes in Russian tundra using the closed chamber method and extrapolated their results to a 114 km² catchment using a classified Landsat TM image (seven vegetation classes). While they recognized large uncertainties associated with spatial and temporal variability, these results were further extrapolated to the entire European part of the Russian tundra, i.e. measurements from 0.36 m^2 plots were extrapolated to 205,000 km^2 but can not be verified. Bubier *et al.* (2005) also used Landsat TM images to scale point measurements from wetland and upland soils near Thompson, Manitoba, to a 1350 km^2 landscape but compared classification results to classified higher-resolution CASI images. Their work includes a detailed discussion of the uncertainties and they note that most remote sensing images cannot identify the sometimes very small areas of extremely high emissions. Since these small emission hot spots tend to be studied preferably during small-scale investigations, scaling results may be inaccurate if the underlying classification is not capable of resolving the small-scale heterogeneity.

Roulet *et al.* (1994) on the other hand, were able to compare extrapolated point measurements (based on Landsat TM) with airborne eddy correlation measurements. Their extrapolated mean flux of 20 ± 16 mg m^{-2} d^{-1} in the Hudson Bay Lowlands was very similar to our landscape scale flux and was found to be within 10% of the airborne observations on the larger scale. Bartlett *et al.* (1992) measured methane flux by closed chamber in a nested design during NASA's ABLE 3A project and were able to compare their results with eddy covariance measurements by Fan *et al.* (1992). Their results agreed well within 200 m of the tower but differences between the methods appeared when a larger area was considered. These differences were attributed to spatial heterogeneity and interhabitat mixing in the classifications.

Thus, up-scaling methane emissions from point measurements or deriving globally valid statements on methane dynamics based on very small-scale studies are not recommended, unless high-resolution classifications able to capture the small-scale heterogeneity of tundra landscapes are available in conjunction with either very detailed spatial measurements in every class or the ability to check upscaled results against real data, such as in a nested design. The latter would also allow for the detection of sources or sinks overlooked in point measurement sampling designs.

In addition to the “measure and multiply” way of upscaling results, process-based models are often used to estimate methane emissions on large scales. However, these models (e.g. Walter 1998, Walter and Heimann, 2001) have mostly been developed on the basis of closed chamber data or other small-scale investigations and are often not able to adequately reproduce larger-scale measurements such as from eddy covariance (R. Petrescu, personal communication; Y. Zhang, personal communication). To adequately represent the different processes that operate on the different scales, these models may need to be revised to incorporate new findings from eddy covariance or other non-intrusive techniques operating on larger scales.

7. Conclusions

The nested approach applied to measurements in this study allowed us to compare results from two scales and to identify some important differences between these two scales. Closed chamber fluxes were roughly an order of magnitude higher in wet polygon centers than on drier rims or in high-center polygons but are only found on 10% of the total area. Depending on weather conditions, the extremely low fluxes from drier sites can end up determining the overall ecosystem flux, because controls and dynamics vary strongly between these two scales.

This heterogeneity, not just in the source strengths of the polygonal tundra but also in terms of controls and seasonal dynamics constitutes a major source of uncertainty for up-scaling exercises, where aggregated results for larger scales cannot be checked against measurements on that scale. Thus, extrapolation should probably be restricted to the next scale up and should in any case be based on remote sensing imagery capable of resolving the small-scale heterogeneity that determines the overall emission. At key sites, integrated multi-scale measurements in a nested design that allows for comparison of scaled emissions and measurements could help identify generally valid scaling procedures.

The uncertainties in matching measurements of extremely heterogeneous measurands on different scales using different techniques, especially in highly complex environments, demonstrate that a new method able to estimate spatial contributions to the net ecosystem flux directly from the larger scale measurements would be desirable.

Acknowledgements

We would like to thank the members of the joint Russian-German expedition LENA-2006, especially Waldemar Schneider (Alfred Wegener Institute), Dmitry Yu. Bolshianov (Arctic and Antarctic Research Institute, St. Petersburg), Mikhail N. Grigoriev (Permafrost Institute, Yakutsk), Alexander Y. Derevyagin (Moscow State University), and Dmitri V. Melnitschenko (Hydro Base, Tiksi) for all logistical, travel, and administrative arrangements. Merten Minke kindly provided the detailed vegetation cover. We are also grateful to Günther "Molo" Stoof for technical support in the field and to Peter Schreiber for help with Figure 3. We greatly appreciate support from Eva-Maria Pfeiffer, Barnim Thees, and Sina Muster on various aspects of this study, as well as thoughtful comments from all internal and anonymous reviewers that helped improving the manuscript.

References

Abramova E, Vishnyakova I, Sachs T (2007) Hydrobiological investigations in the Lena Delta. In: *Russian-German Cooperation SYSTEM LAPTEV SEA: The Expedition LENA 2006, Reports on Polar and Marine Research,* **566** (eds Boike J, Bolshiyanov DY, Gigoriev MN), pp. 6-8. Alfred-Wegener-Institut, Bremerhaven, Germany.

Arrhenius S (1909) *Theorien der Chemie, Nach Vorlesungen gehalten an der Universität von Kalifornien zu Berkeley*. Akademische Verlagsgesellschaft m.b.H., Leipzig, Germany.

Bellisario LM, Bubier JL, Moore TR, Chanton JP (1999) Controls on CH4 Emissions From a Northern Peatland. *Global Biogeochemical Cycles*, **13**, 81–91.

Boike J, Hinzman L, Overduin P, Romanovsky V, Ippisch O, Roth K (2003) A comparison of snow melt at three circumpolar sites: Spitsbergen, Siberia, Alaska. In: *Permafrost: Proceedings of the 8th International Conference on Permafrost 2003* (eds Arenson L, Phillips M, Springman SM), pp. 79-84, Balkema Publishers, Lisse.

Boike J, Wille C, Abnizova A (2008) Climatology and summer energy and water balance of polygonal tundra in the Lena River Delta, Siberia. *Journal of Geophysical Research*, **113,** G03025.

Bubier JL (1995) The Relationship of Vegetation to Methane Emission and Hydrochemical Gradients in Northern Peatlands. *The Journal of Ecology*, **83**, 403-420.

Bubier JL, Moore TR (1994) An ecological perspective on methane emissions from northern wetlands. *Trends in Ecology & Evolution*, **9**, 460-464.

Christensen T, Jonasson S, Callaghan T, Havstrom M (1995) Spatial Variation In High-Latitude Methane Flux Along A Transect Across Siberian And European Tundra Environments. *Journal of Geophysical Research*, **100**, 21035-21045.

Christensen T, Jonasson S, Michelsen A, Callaghan T, Havstrom M (1998) Environmental controls on soil respiration in the Eurasian and Greenlandic Arctic. *Journal of Geophysical Research*, **103**, 29015-29021.

Conrad R (1989) Control of methane production in terrestrial ecosystems. In: *Exchange of Trace Gases between Terrestrial Ecosystems and the Atmosphere* (eds Andreae MO, Schimel DS), pp. 39-58. John Wiley and Sons, Chichester, UK.

Fan SM, Wofsy SC, Bakwin PS *et al.* (1992) Micrometeorological measurements of CH4 and CO2 exchange between the atmosphere and subarctic tundra. *Journal of Geophysical Research*, **97***,* 16627-16643.

Fox AM, Huntley B, Lloyd CR, Williams M, Baxter R (2008) Net ecosystem exchange over heterogeneous Arctic tundra: Scaling between chamber and eddy covariance measurements. *Global Biogeochemical Cycles*, **22**, GB2027.

Friborg T, Christensen T, Hansen B, Nordstroem C, Soegaard H (2000) Trace gas exchange in a high-arctic valley 2. Landscape CH4 fluxes measured and modeled using eddy correlation data. *Global Biogeochemical Cycles*, **14**, 715-723.

Grigoriev NF (1960) The temperature of permafrost in the Lena delta basin – deposit conditions and properties of the permafrost in Yakutia. *Yakutsk*, **2**, 97-101.

Hargreaves K, Fowler D, Pitcairn C, Aurela M (2001) Annual methane emission from Finnish mires estimated from eddy covariance campaign measurements. *Theoretical and Applied Climatology*, **70**, 203-213.

Joabsson A, Christensen T (2001) Methane emissions from wetlands and their relationship with vascular plants: an Arctic example. *Global Change Biology*, **7**, 919-932.

Keppler F, Hamilton JTG, Braß M, Rockmann T (2006) Methane emissions from terrestrial plants under aerobic conditions. *Nature*, **439**, 187-191.

King J, Reeburgh W, Regli S (1998) Methane emission and transport by arctic sedges in Alaska: Results of a vegetation removal experiment. *Journal of Geophysical Research*, **103**, 29083-29092.

King J, Reeburgh W, Thieler K, Kling G, Loya W, Johnson L, Nadelhoffer K (2002) Pulse-labeling studies of carbon cycling in Arctic tundra ecosystems: The contribution of photosynthates to methane emission *Global Biogeochemical Cycles*, **16**, 1062.

Kulmala L, Launiainen S, Pumpanen J, Lankreijer H, Lindroth A, Hari P, Vesala T (2008) H2O and CO2 fluxes at the floor of a boreal pine forest. *Tellus B*, **60**, 167-178.

Kutzbach L (2006) The exchange of energy, water and carbon dioxide between wet arctic tundra and the atmosphere at the Lena River Delta, Northern Siberia. *Reports on Polar and Marine Research,* **541**, Alfred-Wegener-Institut, Bremerhaven, Germany.

Kutzbach L, Schneider J, Sachs T *et al.* (2007) CO2 flux determination by closed-chamber methods can be seriously biased by inappropriate application of linear regression. *Biogeosciences*, **4**, 1005-1025.

Kutzbach L, Wagner D, Pfeiffer EM (2004) Effect of microrelief and vegetation on methane emission from wet polygonal tundra, Lena Delta, Northern Siberia. *Biogeochemistry*, **69**, 341-362.

Kutzbach L, Wille C, Pfeiffer EM (2007) The exchange of carbon dioxide between wet arctic tundra and the atmosphere at the Lena River Delta, Northern Siberia. *Biogeosciences*, **4**, 869-890.

Liebner S, Wagner D (2007) Abundance, distribution and potential activity of methane oxidizing bacteria in permafrost soils from the Lena Delta, Siberia. *Environmental Microbiology*, **9**, 107-117.

Mastepanov M, Sigsgaard C, Dlugokencky EJ, Houweling S, Strom L, Tamstorf MP, Christensen TR (2008) Large tundra methane burst during onset of freezing. *Nature*, **456**, 628-630.

Morrissey LA, Zobel DB, Livingston GP (1993) Significance of stomatal control on methane release from Carex-dominated wetlands. *Chemosphere*, **26**, 339-355.

Nakano T, Kuniyoshi S, Fukuda M (2000) Temporal variation in methane emission from tundra wetlands in a permafrost area, northeastern Siberia. *Atmospheric Environment*, **34**, 1205-1213.

Reeburgh W, King J, Regli S, Kling G, Auerbach N, Walker D (1998) A CH4 emission estimate for the Kuparuk River basin, Alaska. *Journal of Geophysical Research*, **103**, 29005-29013.

Riutta T, Laine J, Aurela M *et al.* (2007) Spatial variation in plant community functions regulates carbon gas dynamics in a boreal fen ecosystem. *Tellus B*, **59**, 838-852.

Sachs T, Wille C, Boike J, Kutzbach L (2008) Environmental controls on ecosystem-scale CH4 emission from polygonal tundra in the Lena River Delta, Siberia. *Journal of Geophysical Research*, **113**, G00A03.

Schimel J (1995) Plant transport and methane production as controls on methane flux from arctic wet meadow tundra. *Biogeochemistry*, **28**, 183-200.

Schneider J, Grosse G, Wagner D (2009) Land cover classification of tundra environments in the Arctic Lena Delta based on Landsat 7 ETM+ data and its application for upscaling of methane emissions. *Remote Sensing of Environment*, **113**, 380-391.

Schuchard-Ficher C, Backhaus K, Humme U, Lohrberg W, Plinke W, Schreiner W (1982) *Multivariate Analysemethoden. Eine anwendungsorientierte Einführung*. Springer, Berlin, Heidelberg, New York.

Schwamborn G, Rachold V, Grigoriev MN (2002) Late Quaternary sedimentation history of the Lena Delta. *Quaternary International*, **89**, 119-134.

Soil Survey Staff (1998) *Keys to Soil Taxonomy 8th Edition*. Pocahontas, Blacksburg, Virginia, USA.

Spott O (2003) *Frostmusterbedingte Seen der Polygonalen Tundra und ihre Funktion als Quellen atmospärischen Methans*. Unpublished Diploma Thesis, University of Leipzig, Leipzig, Germany, 125 pp.

von Storch J (2004) On statistical dissipation in GCM-climate. *Climate Dynamics*, **23**, 1-15.

Suyker A, Verma S, Clement R, Billesbach D (1996) Methane flux in a boreal fen: Season-long measurement by eddy correlation. *Journal of Geophysical Research*, **101**, 28637-28647.

Wagner D, Kobabe S, Pfeiffer EM, Hubberten H (2003) Microbial controls on methane fluxes from a polygonal tundra of the Lena Delta, Siberia. *Permafrost and Periglacial Processes*, **14**, 173-185.

Walter KM, Zimov SA, Chanton JP, Verbyla D, Chapin FS (2006) Methane bubbling from Siberian thaw lakes as a positive feedback to climate warming. *Nature*, **443**, 71-75.

Wanninkhof R, McGillis WR (1999) A Cubic Relationship Between Air-Sea CO2 Exchange and Wind Speed. *Geophysical Research Letters.*, **26**, 1889-1892.

Whalen SC, Reeburgh WS (1996) Moisture and temperature sensitivity of CH4 oxidation in boreal soils. *Soil Biology and Biochemistry*, **28**, 1271-1281.

Whalen SC, Reeburgh WS (1990) A methane flux transect along the trans-Alaska pipeline haul road. *Tellus B*, **42**, 237-249.

Whalen SC, Reeburgh WS (1988) Methane Flux Time Series for Tundra Environments. *Global Biogeochemical Cycles*, **2**, 399-409.

Whiting G, Chanton J (1993) Primary Production Control of Methane Emission from Wetlands. *Nature*, **364**, 794-795.

Wickland KP, Striegl RG, Neff JC, Sachs T (2006) Effects of permafrost melting on CO2 and CH4 exchange of a poorly drained black spruce lowland. *Journal of Geophysical Research*, **111**, G02011.

Wille C, Kutzbach L, Sachs T, Wagner D, Pfeiffer EM (2008) Methane emission from Siberian arctic polygonal tundra: eddy covariance measurements and modeling. *Global Change Biology*, **14**, 1395-1408.

Zona D, Oechel WC (2008) Continuous measurements of methane fluxes by eddy covariance in the Arctic: Results of a large-scale manipulation of water status at Barrow, Alaska. *Geophysical Research Abstracts*, **10**, EGU2008-A-10980.

Table 1: Species and percent coverage for each 50x50cm closed chamber plot (data provided by Merten Minke, 5 July 2006).

	Polygon 1: wet low-center; early degradation			Polygon 2: well-drained high-center; final stage of degradation			Polygon 3: wet low center; advanced degradation			Polygon 4: inundated low-center; no visible degradation			Polygon 5: polygon rim; no standing water		
Species / plot	1	2	3	1	2	3	1	2	3	1	2	3	1	2	3
Vascular plants															
Astragalus frigidus	-	-	-	-	-	-	-	-	-	-	-	-	0.5	1	1
Carex chordorrhiza	10	8	3	-	-	-	30	10	5	7	7	10	-	-	-
Carex concolor	0.1	1	0.1	2	1	0.5	3	5	10	3	3	3	3	3	5
Comarum palustre	1	1	2	-	-	-	2	5	5	3	3	2	-	-	-
Draba pilosa	-	-	-	-	-	-	-	-	-	-	-	-	-	-	0.1
Dryas punctata	-	-	-	-	0.5	1	-	-	-	-	-	-	1	-	-
Equisetum arvense	-	-	-	-	-	0.1	-	-	-	-	-	-	-	-	-
Hierochloe pauciflora	-	-	-	-	-	0.1	-	-	-	-	-	-	-	-	-
Lagotis	-	-	-	0.1	-	-	-	-	-	-	-	-	-	-	-
Parrya nudicaulis	-	-	-	-	-	-	-	-	-	-	-	-	0.1	-	-
Poa arctica	-	-	-	0.1	0.1	-	-	-	-	-	-	-	-	0.1	-
Polygonum viviparum	-	-	-	0.1	0.1	0.1	-	-	-	-	-	-	-	-	-
Pyrola rotundifolia	-	-	-	-	-	-	-	-	-	-	-	-	0.1	0.5	2
Salix glauca or S.reptans	-	-	-	1	0.5	0.1	-	-	-	-	-	-	-	-	-
Saussurea sp.	-	-	-	-	-	-	-	-	-	-	-	-	0.1	0.1	0.1
Mosses															
Aulacomnium turgidum	0.5	-	-	0.5	0.5	5	10	10	5	-	-	-	1	-	0.5
Calliergon giganteum	0.1	0.1	0.1	-	-	-	0.1	0.1	0.1	0.1	0.1	-	-	-	-
Drepanocladus cf. vernicosus	-	-	0.1	-	-	-	50*	-	-	-	-	-	-	-	-
Drepanocladus revolvens	-	-	-	-	-	-	40*	85*	95*	-	-	-	-	-	-
Hylocomium splendens	-	-	-	90	80	85	-	-	-	-	-	-	50	30	99
Meesia triquetra	0.5	0.1	0.5	-	-	-	1	3	0.1	-	-	-	-	-	-
Polytrichum cf. alpinum	-	-	-	-	-	-	-	-	-	-	-	-	5	2	0.1
Rhytidium rugosum	-	-	-	-	-	-	-	-	-	-	-	-	40	60	2
Scorpidium scorpioides	99	100	99	-	-	-	-	-	-	100	100	100	-	-	-
Tomentypnum nitens	-	-	-	10	20	5	-	-	-	-	-	-	-	-	-
Lichens															
Cetraria laevigata	-	-	-	-	-	-	-	-	-	-	-	-	0.5	0.1	0.5
Dactylina arctica	-	-	-	-	-	-	-	-	-	-	-	-	-	0.1	0.5
Peltigera sp.	-	-	-	1	-	5	-	-	-	-	-	-	0.5	1	1
Stereocaulon sp.	-	-	-	-	-	-	-	-	-	-	-	-	-	-	0.1

Table 2: Results of the error-weighted linear regressions given by y = *a* + *b*x.

Polygon	Parameter	Value	Error	*t*-value	$p>\|t\|$	[a]LCI	[b]UCI	*R*	[c]R^2_{adj}	[d]*RMSE* (mg m^{-2} d^{-1})
1	*a* (mg m^{-2} d^{-1})	23.165	4.305	5.381	<0.0001	14.435	31.895	0.82	0.66	1.162
	b (°C^{-1})	5.137	0.513	10.015	<0.0001	4.097	6.178			
3	*a* (mg m^{-2} d^{-1})	21.422	3.355	6.386	<0.0001	14.625	28.219	0.85	0.72	1.803
	b (°C^{-1})	7.549	0.425	17.777	<0.0001	6.688	8.409			
4	*a* (mg m^{-2} d^{-1})	22.255	2.280	9.762	<0.0001	17.627	26.883	0.91	0.83	1.330
	b (°C^{-1})	5.957	0.335	17.769	<0.0001	5.277	6.638			

[a]LCI is the lower confidence interval, [b]UCI is the upper confidence level, [c]R^2_{adj} is the adjusted R^2 taking into consideration the number of explanatory variables and [d]*RMSE* is the root mean squared error.

Table 3: Surface classes and average August methane emissions in the eddy covariance footprint. The area-weighted chamber fluxes (total flux) add up to the flux measured by eddy covariance.

Surface class	**Area coverage (%)**	**CH_4 emission ($mg\ m^{-2}\ d^{-1}$)**	**Total flux ($mg\ m^{-2}\ d^{-1}$)**	**Source of emission rate**
Very wet soils (inundated low-center polygons)	10	94.05	9.41	This study
Drier or moderately moist soils (high-center polygons and rims)	62	7.68	4.76	This study
Open water (+ ebullition estim.) (ponds, lakes, cracks)	14	2.37 (+ 4…30)	0.33 (+0.56…4.20)	Spott (2003)
Overgrown water (small ponds, cracks, shores)	14	44.9	6,29	Spott (2003)
Eddy covariance footprint	100	20.58	20.79 (21.35…24.99)	Sachs *et al.* (2008)

Figure 1: (left) Location of the investigation area and vegetation zones in the Arctic (modified after work by UNEP/GRID-Arendal (1996)). **(right)** Location of the study site Samoylov Island in the Lena River Delta (marked by the square (satellite image: Landsat 7 Enhanced Thematic Mapper (on Nimbus 6)+ GeoCover 2000, NASA (Landsat imagery courtesy of NASA Goddard Space Flight Center and U.S. Geological Survey) (Map by G. Grosse, AWI Potsdam))).

Figure 2: Aerial images of the study site. **(left)** Mosaic of aerial images of Samoylov Island taken in August 2007 (Boike *et al.* 2009). **(right)** The central part of Samoylov Island in August 2007. The asterisk marks the position of the micrometeorological tower. The inset shows the closed chamber study area in direct proximity to the tower. The numbers refer to the micro-sites 1-5.

Figure 3: Schematic overview of the dominant micro-sites. From left to right: thermokarst crack (not explicitly covered in this study), high-center polygon (Polygon 2) surrounded by crack or troughs, wet low-center polygon (Polygon 1, 3, and 4), polygon rim (Polygon 5), and pond/lake (not explicitly covered). The dense diagonal hatching from bottom left to top right marks the permafrost. The wider diagonal hatching in the opposite direction shows mineral soil layers within the seasonally thawed active layer and the denser diagonal hatching on the top denotes the organic layer. The water level is represented by the blue line.

Figure 4: Examples for non-linear evolution of CH_4 concentration in the closed chamber headspace for different micro-sites and dates. The exponential fits of the form $c\mathrm{CH_4} = \beta_1 + \beta_2 \exp(\beta_3\, t)$ are also given for each concentration curve.

Figure 5: Meteorological conditions during the measurements campaign. **(top)** hourly wind speed and atmospheric pressure measured at the eddy covariance tower. (bottom) daily precipitation measured at the long-term climate station 700 m south of the closed chamber site, hourly air temperature in 2 m height measured at the eddy covariance tower, and surface temperature calculated from outgoing long-wave radiation using the Stefan-Boltzmann equation.

Figure 6: (left) closed chamber methane fluxes from micro-sites 1–5 (a-e). Black error bars denote the mean of the standard error of each or the six replicate measurements per micro-site. Grey error bars denote the standard deviation of the replicate measurements within a micro-site, providing information about the spatial variability. The grey line shows the modeled fluxes for micro-site 1 (a), 3 (c), and 4 (d). **(right)** water table, active layer depth, and soil temperatures in 1, 10, 20, and where possible 30 cm depth for each of the micro-sites.

Figure 7: Standard-error weighted linear regression models with surface temperature as the best predictor for methane fluxes from polygons 1, 3, and 4.

Figure 8: Comparison of closed chamber vs. eddy covariance methane fluxes and the dominant controls. **(top)** closed chamber methane fluxes from micro-sites 2 and 5 are extremely low and peaks tend to coincide with peaks in the eddy covariance flux time series, which is best predicted by near-surface turbulence u_*. **(bottom)** closed chamber methane fluxes from micro-sites 1, 3, and 4 are at least an order of magnitude larger (left axis) than those from micro-sites 2 and 5 and also several times larger than those obtained by eddy covariance. Their seasonal dynamics do not match that of the eddy covariance time series and the best predictor of these chamber-based fluxes is surface temperature.

Figure 9: Surface classification of a high-resolution aerial image (S. Muster, unpublished data). The white asterisk in the center of the image marks the position of the eddy covariance tower. Open water covers about 14% of the surface, wet areas (inundated polygon centers and overgrown water, separated in table 3) cover 24% of the surface, and moist/dry areas (high-center polygons and rims, combined in table 3) cover 62% of the surface.

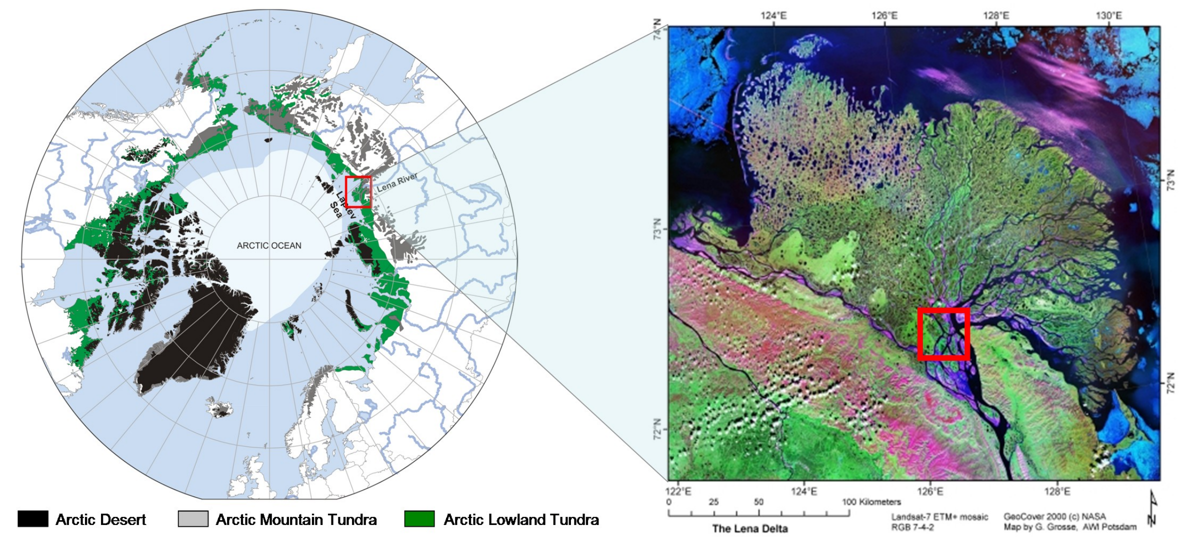
ARCTIC OCEAN
Lena River
Laptev Sea
Arctic Desert
Arctic Mountain Tundra
Arctic Lowland Tundra
124°E
126°E
128°E
130°E
74°N
73°N
72°N
122°E
0 25 50 100 Kilometers
The Lena Delta
Landsat-7 ETM+ mosaic
RGB 7-4-2
GeoCover 2000 (c) NASA
Map by G. Grosse, AWI Potsdam

817

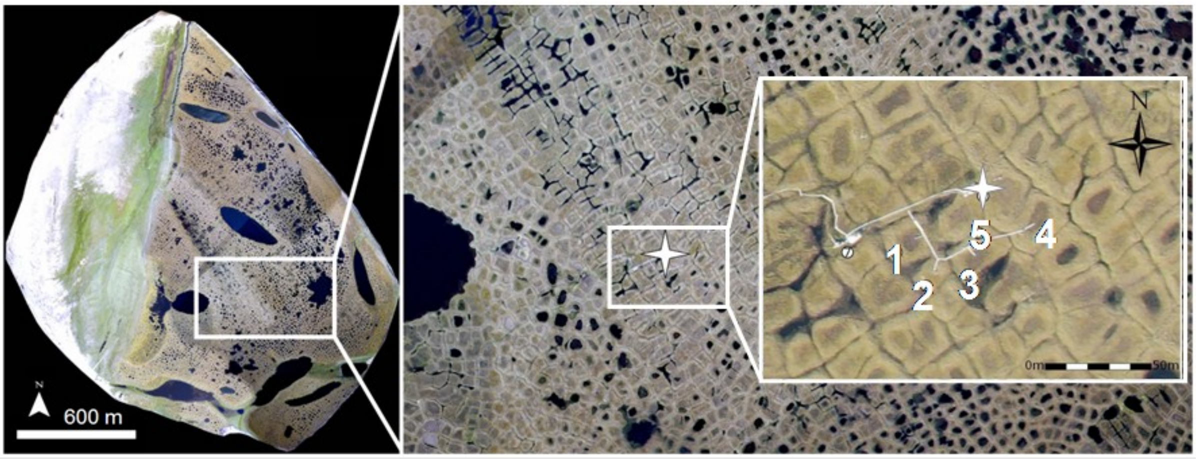

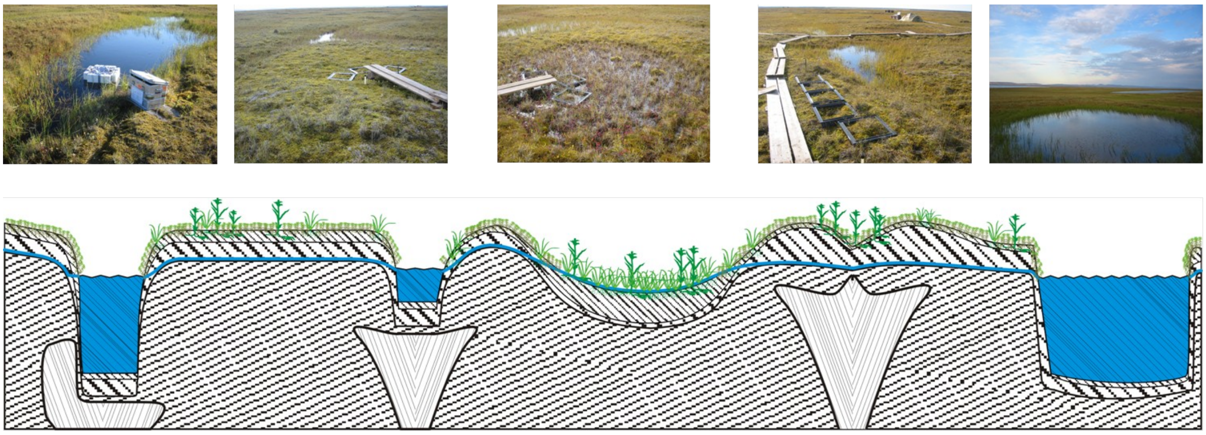

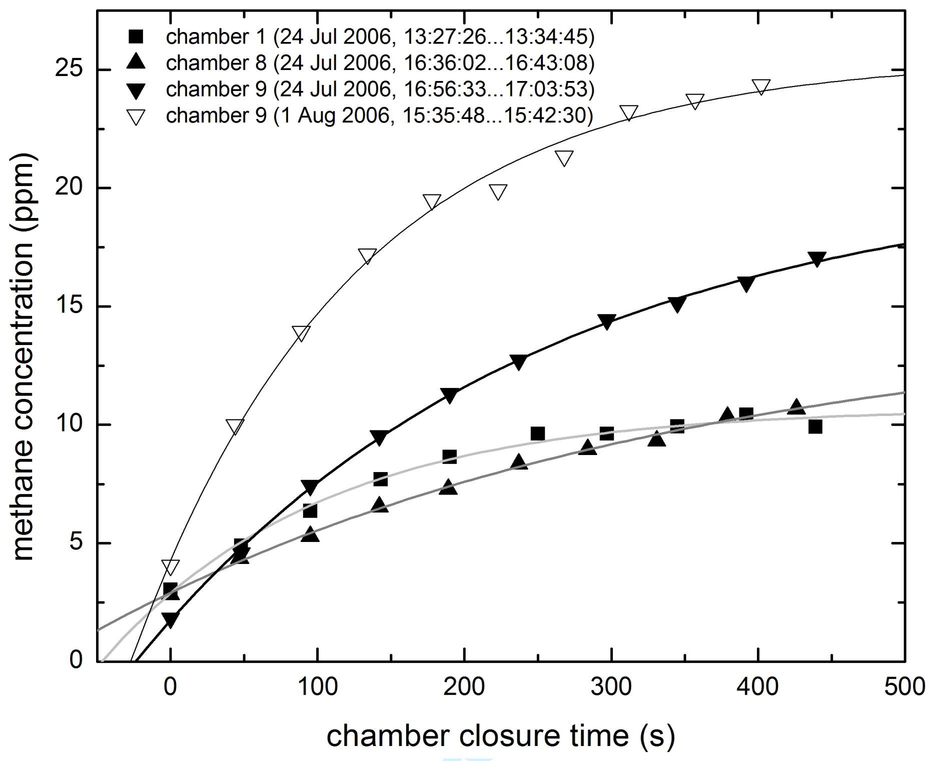
chamber 1 (24 Jul 2006, 13:27:26...13:34:45)
chamber 8 (24 Jul 2006, 16:36:02...16:43:08)
chamber 9 (24 Jul 2006, 16:56:33...17:03:53)
chamber 9 (1 Aug 2006, 15:35:48...15:42:30)
methane concentration (ppm)
0
5
10
15
20
25
0
100
200
300
400
500
chamber closure time (s)

819

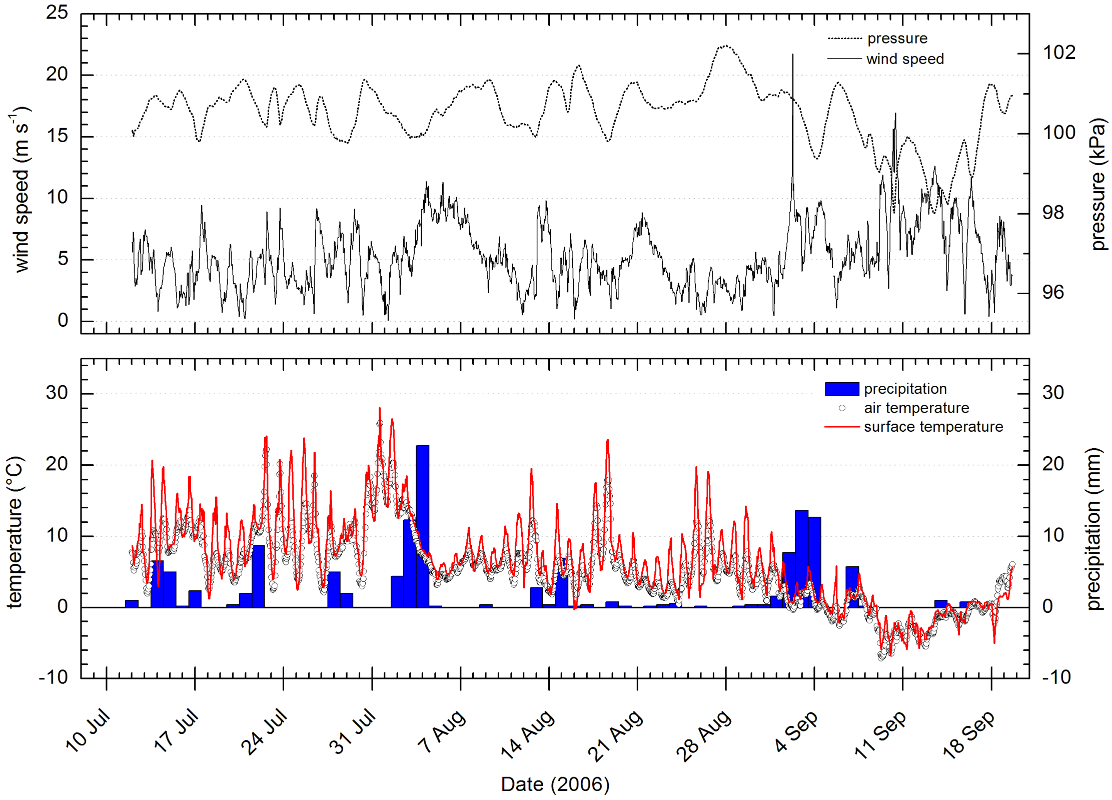
pressure
wind speed
wind speed (m s-1)
pressure (kPa)
precipitation
air temperature
surface temperature
temperature (°C)
precipitation (mm)
10 Jul
17 Jul
24 Jul
31 Jul
7 Aug
14 Aug
21 Aug
28 Aug
4 Sep
11 Sep
18 Sep
Date (2006)

820

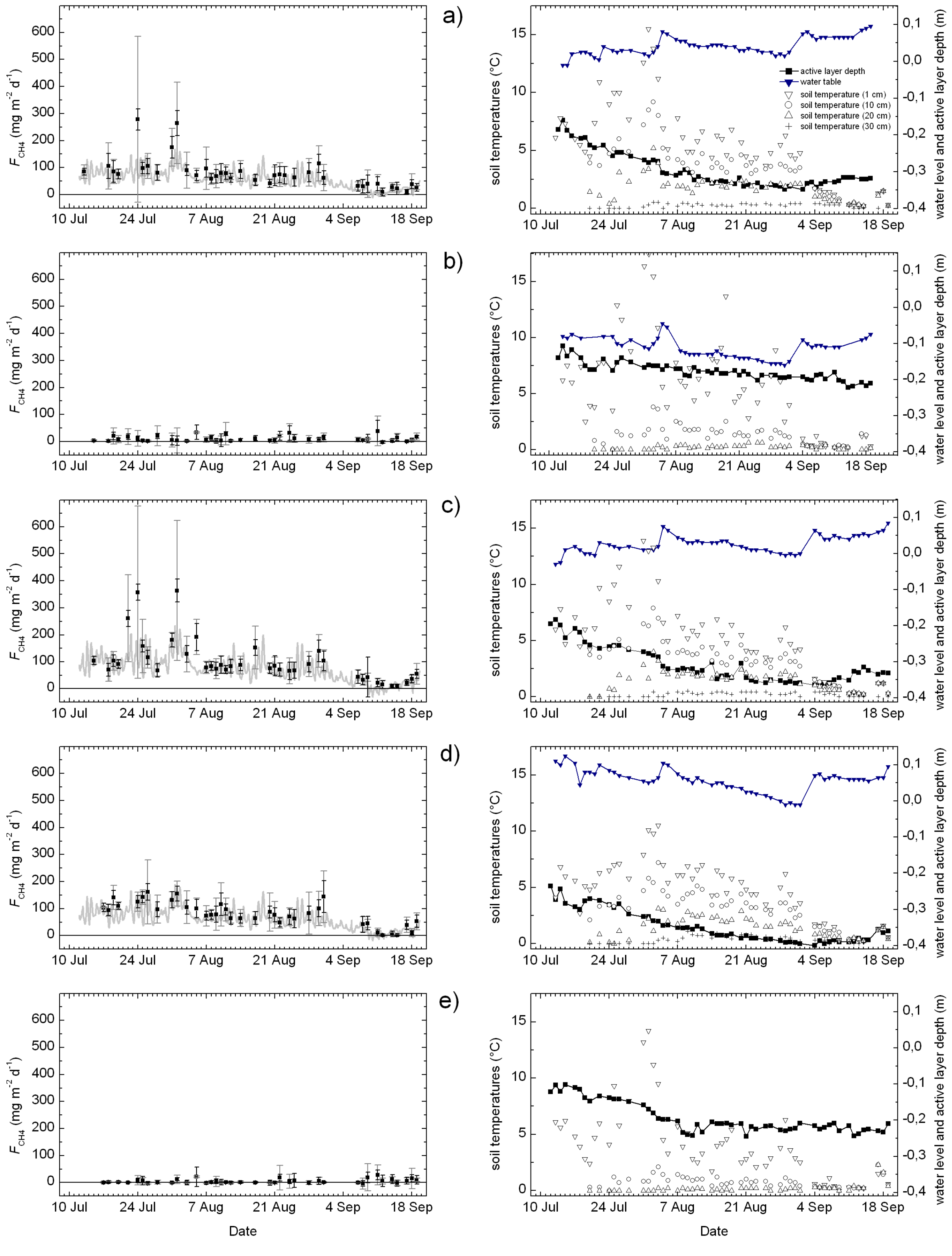
a)
b)
c)
d)
e)
F_{CH4} (mg m^{-2} d^{-1})
soil temperatures (°C)
water level and active layer depth (m)
active layer depth
water table
soil temperature (1 cm)
soil temperature (10 cm)
soil temperature (20 cm)
soil temperature (30 cm)
10 Jul
24 Jul
7 Aug
21 Aug
4 Sep
18 Sep
Date

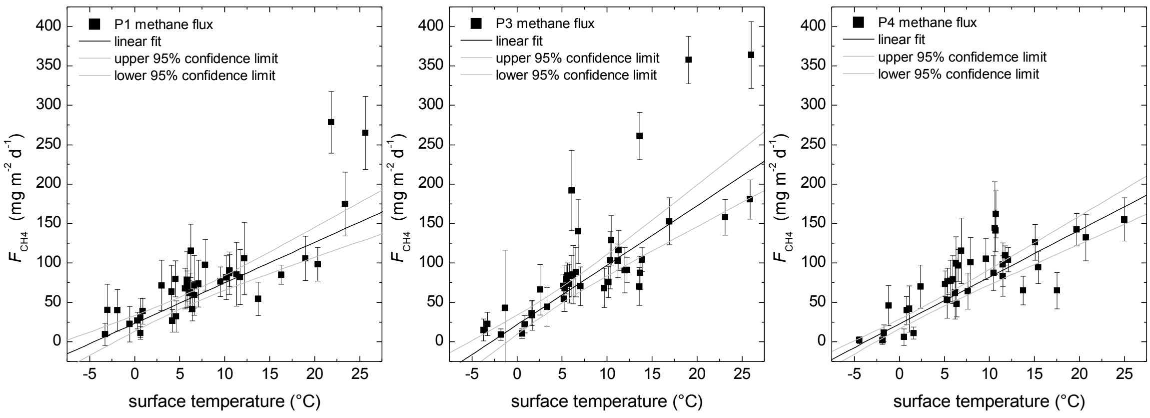
P1 methane flux
linear fit
upper 95% confidence limit
lower 95% confidence limit
P3 methane flux
linear fit
upper 95% confidence limit
lower 95% confidence limit
P4 methane flux
linear fit
upper 95% confidemce limit
lower 95% confidence limit
F_{CH4} (mg m^{-2} d^{-1})
surface temperature (°C)
400
350
300
250
200
150
100
50
0
-5
0
5
10
15
20
25

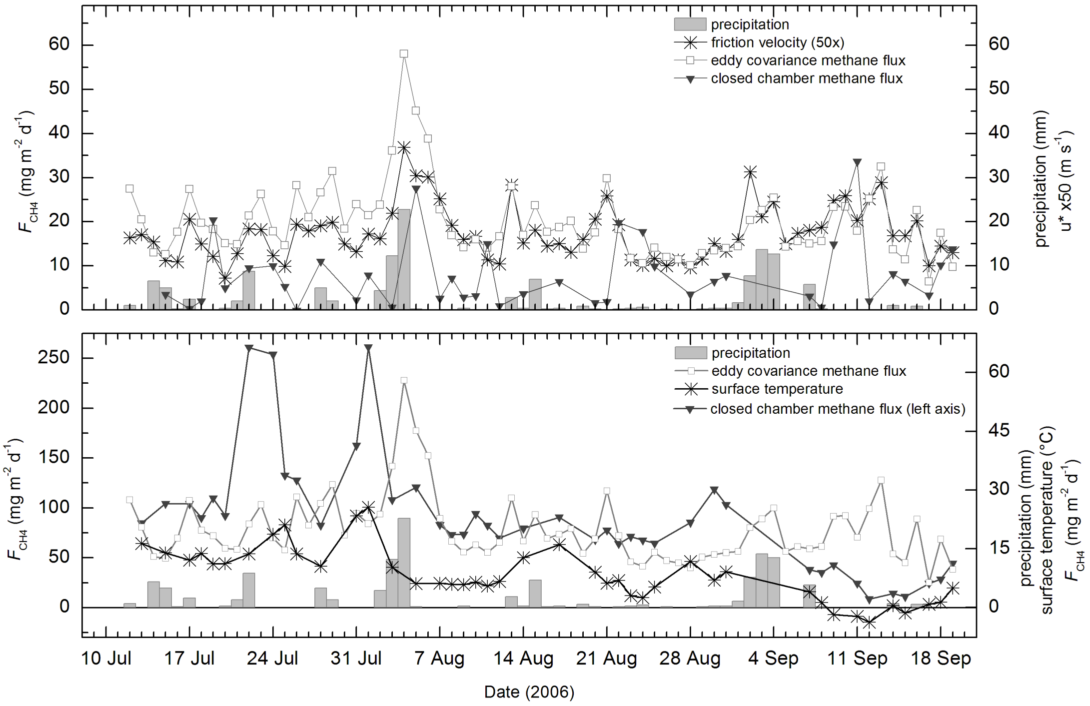
precipitation
friction velocity (50x)
eddy covariance methane flux
closed chamber methane flux
surface temperature
closed chamber methane flux (left axis)
F_{CH4} (mg m^{-2} d^{-1})
precipitation (mm)
u* x50 (m s^{-1})
surface temperature (°C)
10 Jul
17 Jul
24 Jul
31 Jul
7 Aug
14 Aug
21 Aug
28 Aug
4 Sep
11 Sep
18 Sep
Date (2006)

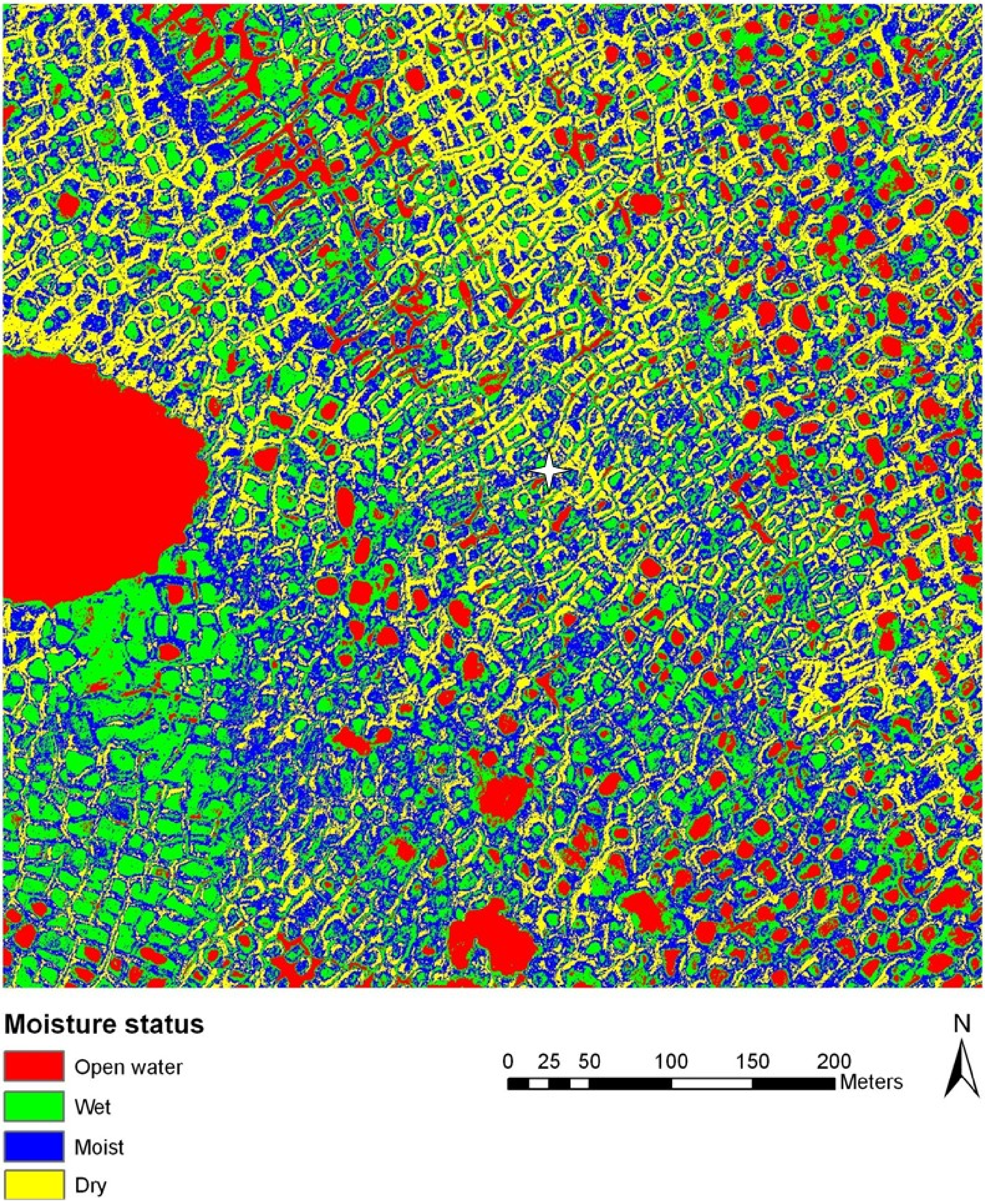
Moisture status
Open water
Wet
Moist
Dry
0 25 50 100 150 200
Meters
N

Environmental controls on CH_4 emission from polygonal tundra on the micro-site scale in the Lena River Delta, Siberia

Torsten Sachs[1,#], Michael Giebels[2, *], Julia Boike[1], Lars Kutzbach[3+]

[1]) Alfred Wegener Institute for Polar and Marine Research, Research Unit Potsdam, Telegrafenberg A43, 14473 Potsdam, Germany

[2]) Institute of Geoecology, Technical University Braunschweig, Langer Kamp 19c, 38106 Braunschweig, Germany

[3]) Institute of Botany and Landscape Ecology, Ernst Moritz Arndt University of Greifswald, Grimmer Str. 88, 17487 Greifswald, Germany

[#])now at: Helmholtz Centre Potsdam – GFZ German Research Centre for Geosciences, Telegrafenberg, 14473 Potsdam, Germany

[*]) now at: Leibniz-Centre for Agricultural Landscape Research, Institute for Landscape Matter Dynamics, Eberswalder Str. 84, 15374 Müncheberg, Germany

[+]) now at: Institute of Soil Science, KlimaCampus, University of Hamburg, Allende-Platz 2, 20146 Hamburg

Corresponding author:

Torsten Sachs, GFZ German Research Centre for Geosciences

Telegrafenberg, 14473 Potsdam, Germany

Phone: +49-331-288-1429

Fax: +49-331-288-1474

Email: torsten.sachs@gfz-potsdam.de

Keywords: Arctic, tundra, methane, permafrost, scaling, closed chambers, eddy covariance

Running title: Controls on tundra CH_4 flux and scaling

Abstract

The carbon budgets of the atmosphere and terrestrial ecosystems are closely coupled by vertical exchange fluxes of carbon dioxide and methane. Uncertainties remain especially with respect to high latitude ecosystems and the processes driving their temporally and spatially highly variable exchange of methane with the atmosphere. To address the problems associated with scaling plot measurements to larger areas in such heterogeneous environments, we conducted intensive field studies on two nested spatial scales in Northern Siberian tundra. Methane fluxes on the micro-site scale (0.1–100 m^2) were measured in the Lena River Delta from July through September 2006 by closed chambers and were compared to simultaneous ecosystem scale (10^4 m^2–10^6 m^2) methane flux measurements by the eddy covariance method at the same study site. Our study adds results from an area that is seriously underrepresented in current efforts to quantify carbon emissions from high latitude ecosystems. Closed chamber measurements of methane fluxes were conducted almost daily on 15 plots in four differently developed polygon centers and on a polygon rim. Controls on methane emission were identified by a stepwise multiple regression procedure. In contrast to the relatively low ecosystem-scale fluxes which were mainly controlled by near-surface turbulence and to a lesser extend by atmospheric pressure and soil temperature, fluxes on the micro-site scale were almost an order of magnitude higher at the wet polygon centers and near zero at the drier polygon rim and a high-center polygon. Micro-site scale methane fluxes varied strongly even within the same micro-sites. The only statistically significant control on chamber-based fluxes was surface temperature calculated using the Stefan-Boltzmann equation in the wet polygon centers, while no significant control was found for the low emissions from the dry sites. The comparison with the eddy covariance measurements reveals differences in both the controls and the seasonal dynamics between the two measurement scales, which may have consequences for scaling and process-based models. However,

despite those differences, closed-chamber measurements from within the eddy covariance footprint could be scaled by an area-weighting approach of landcover classes based on high-resolution imagery to match the total ecosystem-scale emission remarkably well at the investigated polygonal tundra. Our nested sampling design allowed for checking scaling results against measurements and would have enabled us to identify potentially missed sources or sinks.

1. Introduction

In recent decades, methane (CH_4) has increasingly become a focus of studies investigating the carbon cycle and carbon budget as well as the feedback mechanisms increasing greenhouse gas emissions may have on the climate system. Despite these increased efforts, atmospheric concentration data and earth surface emissions still cannot be reconciled, and large uncertainties remain with regard to both mechanistic understanding of methane emissions and the distribution and strength of sources and sinks. Even new sources (Keppler *et al.* 2006; Walter *et al.* 2006) and mechanisms (Mastepanov *et al.* 2008; Sachs *et al.* 2008) are still being identified and discussed. While a general scarcity of data from the Arctic, especially from the extensive Russian tundra areas, is a major factor in this lack of understanding, it is exacerbated by the heterogeneity of the methane sink/source distribution as well as the large variability of methane emissions and the processes controlling these emissions, which vary over different spatial and temporal scales. This heterogeneity contributes to uncertainties in the global methane budget, especially by complicating any attempts at up-scaling emissions from point measurements to larger areas or even global estimates, as small-scale variability can substantially affect the statistics of large-scale variables (von Storch 2004).

Therefore, measurements of methane fluxes and their controls are required on multiple spatial and temporal scales in order to comprehensively understand methane dynamics (Bubier & Moore 1994). At key sites, each measurement should ideally be nested within the footprint of the next larger scale measurements to develop up-scaling methods in small, verifiable steps.

Closed-chamber techniques are widely used for small-scale measurements and allow for good spatial coverage (Whalen & Reeburgh 1990; Christensen *et al.* 1995; Reeburgh *et al.* 1998; Wickland *et al.* 2006). However, they represent an intrusive method and can affect the measured variable even if care is taken to avoid the many potential biases this method is prone to. In a nested approach, results can be checked against other methods such as the eddy covariance technique, thus helping to reduce uncertainties (Fan *et al.* 1992; Riutta *et al.* 2007; Fox *et al.* 2008; Kulmala *et al.* 2008).

We applied such a nested approach in our investigation of methane emissions from northern Siberian wet polygonal tundra in the Lena River Delta. An eddy covariance (EC) system capable of continuous high-resolution methane flux measurements was installed at the site in 2002 and has delivered valuable flux data on the ecosystem scale (Sachs *et al.* 2008; Wille *et al.* 2008). Existing closed chamber sites for studies of the effect of microrelief and vegetation on methane emission (Wagner *et al.* 2003; Kutzbach *et al.* 2004) were located 700 m south of the tower site in an area that was generally drier and more elevated. Thus, in 2005, fifteen closed chambers were installed at five different micro-sites within the eddy covariance footprint and operated simultaneously to the EC system.

The objectives of this paper are to (1) investigate the spatial variability of methane fluxes from wet polygonal tundra within the eddy covariance footprint, (2) identify the dominant processes and controls governing small-scale methane dynamics, (3) compare the results to eddy covariance measurements in order to identify differences or similarities in the seasonal dynamics and the dominant processes and controls.

2. Study area

The study site was located on Samoylov Island near the Russian-German Research Station Samoylov Island, 120 km south of the Arctic Ocean in the southern central Lena River Delta (72°22'N, 126°30'E) (Fig. 1). Samoylov Island is located in the active delta landscape, which covers about 65% of the total 32,000 km² delta. During the past ten years, Samoylov Island has been the focus of a wide range of studies on surface-atmosphere gas and energy exchange, soil science, hydrobiology, microbiology, cryogenesis, and geomorphology (Schwamborn *et al.* 2002; Boike *et al.* 2003, 2008; Kutzbach *et al.* 2004, 2007; Abramova *et al.* 2007; Liebner & Wagner 2007; Sachs *et al.* 2008; Wille *et al.* 2008).

Samoylov Island covers an area of about 5 km². The western part of the island (2 km²) is a modern floodplain with elevations from 1 to 5 meters above sea level (a.s.l.), which is flooded annually during river break-up. The study site is located in the center of the eastern part of the island (3 km²) with elevations from 10 to 16 meters a.s.l. which is composed of sediments of a Late-Holocene river terrace (Fig. 2). The surface of the terrace is characterized by wet polygonal tundra with a flat mesorelief and a pronounced regular micro-relief caused by the development of low-center ice wedge polygons. The typical elevation difference between depressed polygon centers and elevated polygon rims is up to 0.5 m (Kutzbach 2006). The poorly drained and hence mostly inundated centers are characterized by *Typic Historthels*, while *Glacic* or *Typic Aquiturbels* dominate at the dryer but still moist polygon rims (Soil Survey Staff 1998; Kutzbach *et al.* 2004). As the summer progresses, these soils typically thaw to a depth of 30 cm to 50 cm. Hydrophytic sedges as well as mosses dominate the vegetation in the wet polygon centers (Kutzbach *et al.* 2004). Polygon rims are dominated by mesophytic dwarf shrubs, forbs, and mosses. Surface classification of aerial photographs shows that elevated and dryer areas cover approximately 62% of the tundra surrounding the study site, while depressed and wet polygon centers and troughs cover only about 10%. Open and overgrown water makes up 28% of the area (Schneider *et al.* 2009).

The climate in the region is arctic continental climate characterized by very low temperatures and low precipitation. Mean annual air temperature at the meteorological station on Samoylov Island was –14.7°C and mean summer rainfall was 137 mm, ranging from 72 mm to 208 mm in a period from 1999 to 2005 (Boike *et al.* 2008b). Meteorological conditions can change rapidly throughout the growing season depending on the prevailing synoptic weather conditions, which cause either advection of cold and moist air from the Arctic Ocean or warm and dry air from continental Siberia, respectively. The region experiences polar day from 7 May to 8 August and polar night from 15 November to 28 January. Snowmelt and river break-up typically start in the first half of June, and the growing season usually lasts from around mid-June to the first half of September. The continuous permafrost in the delta reaches depths of 500 to 600 meters (Grigoriev 1960) and is characterized by very low temperatures with the top-of-permafrost temperature on Samoylov being approximately –10°C (Boike *et al.* 2003).

3. Investigation sites

Five different micro-sites (four polygons and a rim) characteristic of the prevalent surface and vegetation features in the eddy covariance fetch were established within 40 m of the EC tower and equipped with boardwalks, wells for water level measurements, and three chamber collars each (Fig. 2).

Polygon 1 was a low-center polygon with standing water in the center. The northern side of the polygon rim showed signs of beginning degradation, which might serve as a hydraulic connection to surrounding polygon troughs. Polygon 2 was a high-center polygon with no standing water in the center due to drainage into surrounding thermokarst cracks and troughs. Polygon 3 was a low-center polygon with a massive rim on the western side and a completely degraded rim on the eastern side, where a large thermokarst crack of more than 2 m depth was located. There was standing water in the polygon center throughout most of the growing season. Polygon 4 was a low-center polygon with no apparent rim degradation and no apparent hydraulic connection to surrounding cracks or troughs. It usually maintained the highest water level of all investigated polygon centers. The polygon rim micro-site was underlain by a massive ice wedge and draining into polygon 3 to the east and the crack.

A detailed vegetation cover is given in Table 1 (data provided by M. Minke, 2006). While many species are typical for a rich fen, the polygonal tundra is not a classical fen. Ultimately, all water in polygon centers is provided by rain or snow. However, some of that water also drains into polygon centers from surrounding rims. Nutrient input may be from dust storms and otherwise from fluvial sediments through upward migration into polygon rims due to cryoturbation. Base saturation and pH are relatively high, however, in comparison to active flood plains, the polygonal tundra terrace is rather nutrient limited. A schematic overview and exemplary photographs of the dominant micro-site types are given in Figure 3. The organic layer is about 5 cm thick on polygon rims and about 30 cm in polygon centers.

The root density is high within the top 15 cm of the soil and then decreases towards deeper horizons. At our site, the active layer is deeper in low-center polygons (up to 40 cm) than on polygon rims and high-center polygons (about 20 cm). At the climate station 700 m south of the closed chamber sites, this relationship is reversed with a deeper active layer at the top of the polygon rims than in the centers. Generally, a measurable water table is only present in low-center polygons, but high-center polygons and rims remain very moist at least right above the permafrost table as indicated in the figure. Temperature gradients are generally steeper in rims and high-center polygons, which also reach higher surface temperatures than water-inundated low-center polygons. The CH_4 concentration in the non-inundated soil is close to ambient in the aerobic soil horizons and increases strongly just above the permafrost table, where anaerobic conditions dominate (S. Liebner, personal communication).

4. Methods

4.1. Closed chamber set-up and measurements

Three 50 cm x 50 cm PVC chamber collars with a water-filled channel as a seal were installed in each of the four polygon centers and along the rim and inserted 10-15 cm into the active layer. Chambers were made of opaque PVC and clear PVC, respectively, for light and dark measurements. Chamber volume was 12.5 l at the high-center and rim micro-sites and 37.5 l at the other sites where higher vegetation did not allow for the use of small chambers.

Manual chamber measurements at all 15 plots were made almost daily from 13 July through 19 September 2006 with both clear and opaque chambers, resulting in 6 measurements per day and micro-site. Sample air was drawn from a port on top of the chamber every 45 s for eight to ten minutes for simultaneous analysis of CO_2, CH_4, and water vapor using a photo-acoustic infrared gas spectrometer Innova 1412 with optical filters UA0982 for CO_2, UA0969 for CH_4, and SB0527 for water vapor (INNOVA AirTech Instruments, Denmark). A membrane pump was connected to two other ports and circulated chamber headspace air through perforated dispersive tubes for mixing.

Because of water interference with the CH_4 optical filter, sample air was dried prior to entering the analyzer using 0.3 nm molecular sieve (beads, with moisture indicator; Merck KGaA, Darmstadt, Germany). Temperature and pressure inside the chamber were logged continuously by a MinidanTemp 0.1° temperature logger (Esys GmbH, Berlin, Germany) and the Innova 1412, respectively.

Additional variables measured at the eddy covariance system and an automated long-term monitoring station 700 m south of the EC tower include air temperature, relative humidity, incoming and outgoing solar and infrared radiation, photosynthetically active radiation (PAR), barometric pressure, precipitation, and hourly soil temperatures at 1 cm, 5 cm, 10 cm, 20 cm, 30 cm, and 40 cm depth in a polygon center, as well as in 5 cm depth intervals at a polygon rim.

Manual measurements at each micro-site during chamber deployment included thaw depth using a steel probe, soil temperatures in 5 cm depth intervals, and water level.

4.2. Non-linear flux calculation

The most widely used method for calculating fluxes from the change of concentration in the chamber headspace over time is by linear regression under the assumption that by keeping chamber closure time short, the concentration change is approximately linear. However, (Kutzbach *et al.* 2007) showed that linear regression is frequently not appropriate based on four sets of closed chamber CO_2 data, including those gathered during the measurement campaign reported on here. We found the conclusions for the CO_2 data to also hold for CH_4 (e.g. in Fig. 4) and therefore used the non-linear exponential regression model proposed by Kutzbach *et al.* (2007) to describe CH_4 evolution over time in the chamber headspace:

$$c(t) = f_{\exp}(t) + \varepsilon(t) = \beta_1 + \beta_2 \exp(\beta_3\, t) + \varepsilon(t) \qquad (1)$$

where $\varepsilon(t)$ is the residual error at measurement time t.

At the beginning of the measurement, gas fluxes are assumed to be least disturbed by chamber deployment, and thus, the initial slope of the regression curve $f_{\exp}'(t_0) = (\beta_2 \beta_3)$ is used for flux calculation:

$$F_{CH4}(t_0) = \frac{dc}{dt}(t_0)\frac{p\,V}{R\,T\,A} = f'_{\exp}(t_0)\frac{p\,V}{R\,T\,A} = \beta_2\,\beta_3\frac{p\,V}{R\,T\,A} \qquad (2)$$

where p is air pressure, R is the ideal gas constant, T is the temperature (in Kelvin) and V and A are the volume and basal area of the chamber.

Calculated fluxes were thoroughly screened and all fluxes with a residual standard deviation greater than 0.3 ppm (~ 11 % of the measurements) were excluded from further analysis.

4.3. Model development

Measurements were summarized by averaging the six individual measurements at each micro-site and day. In order to identify statistically significant explanatory variables for the measured methane fluxes, we used multiple linear regressions, starting with a descriptive regression model including all available variables:

$$F_{CH4} = c_0 + c_1 \cdot x_1 + c_2 \cdot x_2 + \ldots + c_n \cdot x_n \qquad (3)$$

We then eliminated all non-significant variables in a stepwise procedure:

First, data were tested for multi-collinearity following Schuchard-Ficher *et al.* (1982). If multi-collinearity was present, variables were dropped until all remaining variables were approximately orthogonal. Next, the residuals of the reduced model were tested for autocorrelation using the Durbin-Watson test (or d-test).

If no autocorrelation was found, the multiple regression coefficient of determination R^2 was tested for significance using the F-test:

$$F(df_1 = q, df_2 = n - q - 1) = \frac{R^2 \cdot (n - q - 1)}{q \cdot (1 - R^2)} \qquad (4)$$

where df indicates degrees of freedom, n is the number of data points and q is the number of predictor variables.

If R^2 was significant, the correlation coefficients c (i = 1,2,…,n) were tested for significance using the t-test. The reduced model that passes these tests provides predictors of the methane flux with a statistically significant explanatory power, i.e. it identifies not necessarily the best fit to the data but the significant and most likely process drivers.

After the parameter selection process, the resulting regression model was fitted to the means of the six replicate measurements per day and micro-site using the inverse square of the mean standard error of these six measurements as a weight, such that points with large errors were given less weight in the fitting process. Cumulative CH_4 fluxes over the measurement period were calculated by integrating the modeled hourly flux time series. The uncertainty of the cumulative fluxes was assessed by error propagation using the RMSE of the regression models as uncertainty indicator for the hourly modeled flux values.

257 # 5. Results

258 ## 5.1. Meteorology

259 At the beginning of the measurement period, air temperatures had just dropped from a
260 daytime summer record of up to 28.9°C on 11 July (mean 18.3°C, minimum 8.9°C) to well
261 below 10°C (Fig. 5). Fluctuations between daytime and nighttime temperatures were strong
262 throughout July with mean temperatures rising from 8.4°C in the first week of measurements
263 to 12.2°C in the third week. The maximum daily mean temperature during the measurements
264 period was reached on 31 July at 18.5°C. A storm system with heavy precipitation of up to 23
265 mm per day and prolonged periods of mean hourly wind speeds around 10 m s^{-1} caused daily
266 mean temperatures to drop sharply to as low as 4.2°C in the first week of August. Mean daily
267 temperatures never exceeded 11.9°C for the remaining season and remained between 2.3°C
268 and 11.9°C during August. Another storm system in the first week of September yielded 34
269 mm of precipitation within three days and wind speeds exceeding 20 m s^{-1}. Temperatures
270 continued to decrease and reached a daily minimum at –5.2°C on 9 September. Mean daily
271 temperature was well below zero for the entire week from 8 September to 15 September and
272 caused the mean September temperature (1 September – 19 September) to be below freezing
273 despite increasing temperatures during the last week of the measurement period. The second
274 week of September was characterized by extremely low atmospheric pressure (down to 98
275 kPa) and frequent snow storms with wind speeds above 10 m s^{-1}. Snow started to accumulate
276 on 12 September and reached depths of 8–10 cm in polygon centers and 2–6 cm on elevated
277 areas, but all snow had disappeared on 18 September after advection of warmer air from the
278 south. By mid-September, all water bodies except for the large thermokarst lakes were
279 covered with ice up to 8 cm thick and soils were frozen up to approximately 10 cm depth.
280 Long-term temperature data are available from Tiksi, which is located 110 km south-east of
281 Samoylov Island but characterized by very similar temperatures. Temperature conditions in

2006 were within ±1°C of the long-term average in July (7°C), August (7°C), and September (1°C). The average daily wind speed was 5.3 ms^{-1} during the study period, which is 0.6 ms^{-1} higher than in 2003 and 2004 (Kutzbach 2006). Winds from east southeast were clearly predominant, but west-northwesterly and southern winds also occurred frequently (data not shown).

5.2. Methane fluxes and controls

Fluxes were averaged across six measurements per micro-site and day (two measurements on each of three plots per micro-site) and are reported with the standard deviation as a measure of within-site spatial variability and the averaged standard error of the measurements (Fig. 6, table 2).

At the wet and low-centered Polygons 1, 3, and 4, the methane fluxes were highest and showed a clear seasonal trend, with the occurrence of the highest fluxes at the end of July followed by a decrease towards the frost period at the middle of September. During most times, water levels were above the soil surface in these polygons, only at the end of August did they come close to, or dropped slightly below, the soil surface. The active layer depth increased from between 18 and 24 cm at the beginning of the measurement period to a maximum of between 35 and 40 cm, which was reached on 4 September. After this time, refreezing from the bottom decreased the active layer depth at all three sites by about 4 cm until 19 September.

At the relatively “dry” sites 2 (high-centered Polygon) and 4 (polygon rim), the average methane fluxes were smaller by about one order of magnitude compared to wet and inundated low-center polygons and showed no clear seasonal trend. The water level in the high-centered polygon remained slightly above the permafrost table and never reached the surface during the entire measurement period. The active layer depth at both sites increased from about 10 cm to 20 cm during the measurement period.

Typically, the standard error of the measurements was around ± 25 mg m^{-2} d^{-1} for Polygon 1, 3, and 4, and about ± 10 mg m^{-2} d^{-1} for the drier micro-sites. The within-site spatial variability was about ± 43 mg m^{-2} d^{-1} in Polygon 1, 3, and 4, and about ± 10 to 15 mg m^{-2} d^{-1} at the drier sites. Polygon 4 showed less spatial variability than Polygon 1 and 3. Except on the polygon rim, the spatial variability decreased strongly towards the end of the season, most pronouncedly in the low-center polygons.

The regression analysis revealed that it was not possible to construct a multidimensional model with independent and significant parameters. In the resulting one-dimensional model for the low-center polygons 1, 3, and 4, the predictor variable with the highest explanatory power was the surface temperature as calculated using the Stefan-Boltzmann equation (Table 3; Fig. 7). Except for the underestimation of the extreme flux peaks on 24 July and 1 August at Polygon 1 and Polygon 3, the modeled methane flux agreed well with measured fluxes (mean $RMSE$ = 1.43 mg m^{-2} d^{-1}). At Polygons 2 and 5, very low methane concentrations in the closed chamber system frequently resulted in a low signal-to-noise ratio and a high exclusion rate during flux calculation. No statistically significant correlation with any of the observed environmental parameters was found.

6. Discussion

6.1. Environmental controls on micro-site methane emission

Very wet polygon center (micro-sites 1, 3, and 4)

The single parameter with the highest explanatory power for the observed CH_4 fluxes and statistical significance at the three low-center polygon sites was surface temperature. Many studies found relationships between soil temperature in different depths and methane flux (Whalen & Reeburgh 1988; Bubier 1995; Christensen *et al.* 1995; Bellisario *et al.* 1999; Nakano *et al.* 2000), but only few (Hargreaves *et al.* 2001) identified surface temperature as a predictor of methane flux or even measured or calculated it. This finding may be explained by the significantly dampened variability of soil temperatures at our site. A shallow active layer and cold permafrost reduce short-term variability already close below the surface, and thus the highly variable surface temperature is better suited to predict highly variable methane fluxes than soil temperature with little variability, at least on the daily timescale investigated here. While Roulet *et al.* (1992) found significant temperature relationships for only 3 out of 24 sites (beaver ponds and swamp), the slopes of their regression (5.5 mg m^{-2} d^{-1} °C^{-1}, 7.0 mg m^{-2} d^{-1} °C^{-1}, and 7.3 mg m^{-2} d^{-1} °C^{-1}) were similar to the slopes in our relationships (table 3).

Kutzbach *et al.* (2007) also found surface temperature and not soil temperature as the best predictor variable for ecosystem respiration at the same study site, which was explained by the importance of above-ground plant respiration. Vegetation might also explain the controlling influence of surface temperature in this study if surface temperature is seen as an indicator for plant productivity. Vegetation plays an important role in the methane cycle, supplying substrate for methanogens, in some cases (e.g. sedges) oxygen for methanotrophs, and a conduit for methane release to the atmosphere (Morrissey *et al.* 1993; Whiting & Chanton 1993; Bubier 1995; Schimel 1995; King *et al.* 1998, 2002; Bellisario *et al.* 1999; Joabsson & Christensen 2001). At our site, plant-mediated methane transport was found to account for 27 to 66% of overall methane fluxes (Kutzbach *et al.* 2004). We did not find significantly different emission rates between measurements with clear chambers and those with opaque chambers, suggesting that there was no stomatal effect in plant-mediated methane flux.

While methane emission was found to increase with higher water levels in many studies (e.g. Suyker *et al.* 1996; Friborg *et al.* 2000; Wagner *et al.* 2003), there was no correlation between water level and methane emission at our site on the daily time scale. This is considered to be due to the fact that in low-center polygons, where most of the methane was emitted, the water level remained at or above the soil surface at all times and thus fluctuations in water level did not change the ratio of oxic/anoxic soil column. In fact, the dampened methane emission dynamics at Polygon 4, which had the highest water level during the measurement period, suggests that water levels above the surface may actually hinder methane emission by submerging vegetation and presenting a barrier to both soil-diffusive flux and plant-mediated flux. Bellisario *et al.* (1999) also found an inverse relationship between water table and methane flux but did not discuss the finding further. Zona & Oechel (2008) also found that in certain conditions, a drop in water table caused increased methane flux in a large-scale manipulation experiment in Arctic tundra in Barrow, Alaska. However, on the seasonal time scale, the water table explains about 85 % of the spatial variability of methane fluxes at the investigated polygonal tundra (R^2_{adj} = 0.85; n = 5).

Polygon rims & high-center polygons (micro-sites 2 & 5)

Polygon rims and high-center polygons appear to behave similarly despite strongly differing soil conditions (i.e. cryoturbated mineral soils on the rims vs. organic layers and peat in the high-center). No significant predictor was found for the high-center and rim site flux data. The most pronounced effect on methane emission from these sites is expected to be that of precipitation and temporarily rising water levels which shift the distribution of aerobic/anaerobic soil volume towards anaerobic conditions, favoring methane production. At the same time, water percolating into the pore space will displace methane left in those pores and increase the advective flux. The net effect is a transient increase in methane production and emission from these micro-sites during periods of heavy precipitation and transient rises in water levels.

Open water surfaces

Open water surfaces are an important feature of the polygonal tundra and include relatively small but deep thermokarst cracks as well as ponds and larger lakes. Unfortunately, it was only possible to conduct exploratory closed chamber measurements on open water surfaces in this study. More detailed assessments of the water bodies can be found in Spott (2003).

Open water surfaces are mostly affected by increased wind speeds. Diffusive and turbulent gas transfer between water and atmosphere is known to be proportional to the third power of the wind speed (Wanninkhof & McGillis 1999). In addition, storm systems are associated with decreasing atmospheric pressure, which was observed to increase methane flux by ebullition. Spott (2003) measured methane fluxes from water bodies of the polygonal tundra on Samoylov Island by closed chambers and found open water surfaces to emit between 1.9 to 9.9 mg m^{-2} d^{-1} during calm conditions while vegetated areas emitted up to 88.7 mg m^{-2} d^{-1}.

6.2. Comparison of closed chamber vs. eddy covariance methane fluxes and their controls on different scales

Simultaneous eddy covariance measurements of methane flux at the same site are described in Sachs *et al.* (2008) and – in combination with the results reported here – constitute the first study of methane emission from a Siberian arctic tundra site on different but nested scales. The comparison of micro-site fluxes from closed chamber data and ecosystem-scale fluxes of the eddy covariance system (Sachs *et al.* 2008) reveals differences both in terms of the dominant controls on methane flux as well as the seasonal variation of the fluxes (Fig. 8). On the ecosystem scale, no clear seasonal course was visible, although maximum fluxes did occur during the first week of August. On the micro-site scale, however, low-center polygons showed a decrease of methane emission from July to August by about 30% and a pronounced decrease from August to September by 70%, which is more in line with most studies (e. g. Whalen & Reeburgh 1988; Christensen *et al.* 1998; Wagner *et al.* 2003). The drier micro-sites, on the other hand, did not show any seasonal course and thus appear more comparable to the seasonal dynamics on the ecosystem scale.

In addition to the differing seasonal dynamics, peak methane emissions on the different scales did not occur on the same dates. Ecosystems scale emission peaks were usually associated with high wind speed, low atmospheric pressure, and precipitation events, and the best predictor of ecosystem scale methane emission was near-surface turbulence. The very few identifiable peaks at the drier micro-sites also tend to coincide with these weather conditions, while emission peaks at low-center polygons typically occurred during warm and dry days. At the end of the season, methane fluxes on the different scales diverge completely, with ecosystem scale and drier micro-site fluxes increasing during the last week while low-center polygon emissions reached their minima during the frost period.

Surface classification and flux weighting

Surface classification of high resolution aerial images by unsupervised k-means classification in ENVI 4.6 reveals a distribution of these micro-sites which is likely to be wrongly estimated by simple visual assessment in the field: the very wet high methane emission sites only constitute 24% of the area while moderately moist and relatively drier sites occupy 35% and 27%, respectively. Open water without vegetation is present in about 14% of the area (Fig. 9). Based on our knowledge of the site and the associated methane emissions, we merged the moist and relatively dry sites, which correspond to high center polygons and polygon rims, into one class representing 62% of the surface. Similarly, if water with emergent vegetation is classified separately from inundated low-center polygons where water levels are just at or slightly above the surface, the fraction of low-center polygons is reduced to about 10%, while overgrown water covers about 14% of the area. This latter estimate is based on an older supervised classification of the same site by Schneider *et al.* (2009). Table 4 provides typical methane emissions for each surface class and the fraction of the surface it covers during August, when the underlying aerial image was taken. Ebullition fluxes according to Spott (2003) were 3.8 mg m^{-2} d^{-1} on average (measured at three water bodies) but ranged from 0 mg m^{-2} d^{-1} to 30 mg m^{-2} d^{-1}. Adding ebullition flux to the emissions from open water surfaces can change the total flux but would have to be at least three times higher than the diffusive flux to change the total flux estimate by 5% or more.

During periods of precipitation, lower temperatures, and higher wind speeds emissions from low emitting micro-sites (high center polygon and polygon rim) can increase up to five-fold. Even when assuming 20% reduced emissions from very wet soils (compared to August average) and equal emissions from water bodies, increased emissions from drier soils can increase the total ecosystem flux even without the additional emission that can be expected from water bodies due to increased turbulence during (table 4). This thought experiment demonstrates that on a landscape scale, the effects of weather-induced changes in methane emission can easily be the opposite of what is observed on a small scale or expected based on previous (mostly closed chamber) studies.

These differences in results from two distinct spatial scales demonstrate the merit of integrated investigations of methane dynamics on multiple nested scales, and in particular the need for non-intrusive and spatially integrating measurements such as by eddy covariance or airborne instruments, allowing to compare extrapolated results from small scales to actual data on the next larger scale. At key sites, scaled emissions should be checked in small steps to increase confidence and reduce uncertainties in scaling procedures. In this study, closed-chamber measurements from within the eddy covariance footprint could be scaled by an area-weighting approach of landcover classes to match the total ecosystem-scale emission despite the different controls and methane dynamics on the two scales. On the other hand, another upscaling study by Schneider *et al.* (2009) reports total emissions from the same types and distribution of landcover classes that are about 34% lower than in this study. The closed chamber measurements forming the basis of the Schneider *et al.* (2009) upscaling were located 700 m south of the eddy covariance tower in a generally drier and more elevated area (Wagner *et al.* 2003). The classification used in their upscaling, however, was based on two aerial image scenes, both of which cover the wetter area in the center of the island that is also covered by our classification (Fig. 9). If a classification of the actual measurement site results in the same landcover classes, the discrepancy between the two studies implies that either differences in flux calculation from closed chamber data (linear regression in Schneider *et al.* (2009) vs. nonlinear regression here) or spatial heterogeneities cause the significant difference between these two estimates. If differences in the flux calculation caused the discrepancy, this underlines the importance of accurate flux determination as discussed in Kutzbach *et al.* (2007). If spatial heterogeneity is the reason, it demonstrates clearly that small-scale measurements of methane can not readily be applied to scales beyond the "next step" in the scaling ladder. And if the classification of the actual measurement site results in different landcover classes, it emphasizes the importance of obtaining data and information intended to be integrated under as similar conditions as possible.

Difficulties in upscaling emissions governed by highly local controls were already identified by Bubier & Moore (1994) and multiscale studies were recommended. Nonetheless, most studies extrapolate emissions from point measurements with little or no ability to validate results with measurements on the larger scale. Heikkinen *et al.* (2004) measured carbon and methane fluxes in Russian tundra using the closed chamber method and extrapolated their results to a 114 km² catchment using a classified Landsat TM image (seven vegetation classes). While they recognized large uncertainties associated with spatial and temporal variability, these results were further extrapolated to the entire European part of the Russian tundra, i.e. measurements from 0.36 m^2 plots were extrapolated to 205,000 km^2 but can not be verified. Bubier *et al.* (2005) also used Landsat TM images to scale point measurements from wetland and upland soils near Thompson, Manitoba, to a 1350 km^2 landscape but compared classification results to classified higher-resolution CASI images. Their work includes a detailed discussion of the uncertainties and they note that most remote sensing images cannot identify the sometimes very small areas of extremely high emissions. Since these small emission hot spots tend to be studied preferably during small-scale investigations, scaling results may be inaccurate if the underlying classification is not capable of resolving the small-scale heterogeneity.

Roulet *et al.* (1994) on the other hand, were able to compare extrapolated point measurements (based on Landsat TM) with airborne eddy correlation measurements. Their extrapolated mean flux of 20 ± 16 mg m^{-2} d^{-1} in the Hudson Bay Lowlands was very similar to our landscape scale flux and was found to be within 10% of the airborne observations on the larger scale. Bartlett *et al.* (1992) measured methane flux by closed chamber in a nested design during NASA's ABLE 3A project and were able to compare their results with eddy covariance measurements by Fan *et al.* (1992). Their results agreed well within 200 m of the tower but differences between the methods appeared when a larger area was considered. These differences were attributed to spatial heterogeneity and interhabitat mixing in the classifications.

Thus, up-scaling methane emissions from point measurements or deriving globally valid statements on methane dynamics based on very small-scale studies are not recommended, unless high-resolution classifications able to capture the small-scale heterogeneity of tundra landscapes are available in conjunction with either very detailed spatial measurements in every class or the ability to check upscaled results against real data, such as in a nested design. The latter would also allow for the detection of sources or sinks overlooked in point measurement sampling designs.

Process-based models are increasingly used to estimate methane emissions on large scales. However, these models (e.g. Walter 1998, Walter and Heimann, 2001) have mostly been developed on the basis of closed chamber data or other small-scale investigations and therefore rely mostly on the "traditional" drivers of methane emission associated with soil and microbial processes. To our knowledge, the interaction of the atmospheric boundary layer with the soil-vegetation system, in particular the influence of turbulence on methane emissions, is currently not implemented in these models. New findings from eddy covariance or other non-intrusive techniques operating on larger scales may need to be incorporated to adequately represent the different processes that operate on different scales.

7. Conclusions

The nested approach applied to measurements in this study allowed us to compare results from two scales and to identify some important differences between these two scales. Closed chamber fluxes were roughly an order of magnitude higher in wet polygon centers than on drier rims or in high-center polygons but are only found on 10% of the total area. Depending on weather conditions, the extremely low fluxes from drier sites can end up determining the overall ecosystem flux, because controls and dynamics vary strongly between these two scales.

This heterogeneity, not just in the source strengths of the polygonal tundra but also in terms of controls and seasonal dynamics constitutes a major source of uncertainty for up-scaling exercises, where aggregated results for larger scales cannot be checked against measurements on that scale. Thus, extrapolation should be restricted to the next larger scale and should in any case be based on remote sensing imagery capable of resolving the small-scale heterogeneity that determines the overall emission. At key sites, integrated multi-scale measurements in a nested design that allows for comparison of scaled emissions and measurements could help identify generally valid scaling procedures.

The uncertainties in matching measurements of extremely heterogeneous measurands on different scales using different techniques, especially in highly complex environments, demonstrate that a new method able to estimate spatial contributions to the net ecosystem flux directly from the larger scale measurements would be desirable.

532 **Acknowledgements**

533 We would like to thank the members of the joint Russian-German expedition LENA-2006, 534 especially Waldemar Schneider (Alfred Wegener Institute), Dmitry Yu. Bolshianov (Arctic 535 and Antarctic Research Institute, St. Petersburg), Mikhail N. Grigoriev (Permafrost Institute, 536 Yakutsk), Alexander Y. Derevyagin (Moscow State University), and Dmitri V. 537 Melnitschenko (Hydro Base, Tiksi) for all logistical, travel, and administrative arrangements. 538 Merten Minke kindly provided the detailed vegetation cover. We are also grateful to Günther 539 “Molo” Stoof for technical support in the field and to Peter Schreiber for help with Figure 3. 540 We greatly appreciate support from Eva-Maria Pfeiffer, Barnim Thees, and Sina Muster on 541 various aspects of this study, as well as thoughtful comments from all internal and anonymous 542 reviewers that helped improving the manuscript. Lars Kutzbach was supported through the 543 Cluster of Excellence 'CliSAP' (EXC177), University of Hamburg, funded through the 544 German Science Foundation (DFG).

References

Abramova E, Vishnyakova I, Sachs T (2007) Hydrobiological investigations in the Lena Delta. In: *Russian-German Cooperation SYSTEM LAPTEV SEA: The Expedition LENA 2006, Reports on Polar and Marine Research,* **566** (eds Boike J, Bolshiyanov DY, Gigoriev MN), pp. 6-8. Alfred-Wegener-Institut, Bremerhaven, Germany.

Arrhenius S (1909) *Theorien der Chemie, Nach Vorlesungen gehalten an der Universität von Kalifornien zu Berkeley*. Akademische Verlagsgesellschaft m.b.H., Leipzig, Germany.

Bellisario LM, Bubier JL, Moore TR, Chanton JP (1999) Controls on CH_4 Emissions From a Northern Peatland. *Global Biogeochemical Cycles*, **13**, 81–91.

Boike J, Hinzman L, Overduin P, Romanovsky V, Ippisch O, Roth K (2003) A comparison of snow melt at three circumpolar sites: Spitsbergen, Siberia, Alaska. In: *Permafrost: Proceedings of the 8th International Conference on Permafrost 2003* (eds Arenson L, Phillips M, Springman SM), pp. 79-84, Balkema Publishers, Lisse.

Boike J, Bolton B, Grüber M, Langer M, Muster S, Piel K, Sachs T, Stoof G, Westermann S, Scheritz M (2008a) A high resolution orthorectified picture of Samoylov. In: *The Russian-German Cooperation SYSTEM LAPTEV SEA: The Expedition Lena – New Siberian Islands 2007 during the International Polar Year 2007/2008, Reports on Polar and Marine Research,* **584**, (eds Boike J, Bolshiyanov DY, Schirrmeister L, Wetterich S), p. 22. Alfred-Wegener-Institut, Bremerhaven, Germany.

Boike J, Wille C, Abnizova A (2008b) Climatology and summer energy and water balance of polygonal tundra in the Lena River Delta, Siberia. *Journal of Geophysical Research,* **113,** G03025.

Bubier JL (1995) The Relationship of Vegetation to Methane Emission and Hydrochemical Gradients in Northern Peatlands. *The Journal of Ecology*, **83**, 403-420.

Bubier JL, Moore TR (1994) An ecological perspective on methane emissions from northern wetlands. *Trends in Ecology & Evolution*, **9**, 460-464.

Christensen T, Jonasson S, Callaghan T, Havstrom M (1995) Spatial Variation In High-Latitude Methane Flux Along A Transect Across Siberian And European Tundra Environments. *Journal of Geophysical Research*, **100**, 21035-21045.

Christensen T, Jonasson S, Michelsen A, Callaghan T, Havstrom M (1998) Environmental controls on soil respiration in the Eurasian and Greenlandic Arctic. *Journal of Geophysical Research*, **103**, 29015-29021.

Conrad R (1989) Control of methane production in terrestrial ecosystems. In: *Exchange of Trace Gases between Terrestrial Ecosystems and the Atmosphere* (eds Andreae MO, Schimel DS), pp. 39-58. John Wiley and Sons, Chichester, UK.

Fan SM, Wofsy SC, Bakwin PS *et al.* (1992) Micrometeorological measurements of CH_4 and CO_2 exchange between the atmosphere and subarctic tundra. *Journal of Geophysical Research*, **97***,* 16627-16643.

Fox AM, Huntley B, Lloyd CR, Williams M, Baxter R (2008) Net ecosystem exchange over heterogeneous Arctic tundra: Scaling between chamber and eddy covariance measurements. *Global Biogeochemical Cycles*, **22**, GB2027.

Friborg T, Christensen T, Hansen B, Nordstroem C, Soegaard H (2000) Trace gas exchange in a high-arctic valley 2. Landscape CH_4 fluxes measured and modeled using eddy correlation data. *Global Biogeochemical Cycles*, **14**, 715-723.

Grigoriev NF (1960) The temperature of permafrost in the Lena delta basin – deposit conditions and properties of the permafrost in Yakutia. *Yakutsk*, **2**, 97-101. (in Russian).

Hargreaves K, Fowler D, Pitcairn C, Aurela M (2001) Annual methane emission from Finnish mires estimated from eddy covariance campaign measurements. *Theoretical and Applied Climatology*, **70**, 203-213.

Joabsson A, Christensen T (2001) Methane emissions from wetlands and their relationship with vascular plants: an Arctic example. *Global Change Biology*, **7**, 919-932.

Keppler F, Hamilton JTG, Braß M, Rockmann T (2006) Methane emissions from terrestrial plants under aerobic conditions. *Nature*, **439**, 187-191.

King J, Reeburgh W, Regli S (1998) Methane emission and transport by arctic sedges in Alaska: Results of a vegetation removal experiment. *Journal of Geophysical Research*, **103**, 29083-29092.

King J, Reeburgh W, Thieler K, Kling G, Loya W, Johnson L, Nadelhoffer K (2002) Pulse-labeling studies of carbon cycling in Arctic tundra ecosystems: The contribution of photosynthates to methane emission *Global Biogeochemical Cycles*, **16**, 1062.

Kulmala L, Launiainen S, Pumpanen J, Lankreijer H, Lindroth A, Hari P, Vesala T (2008) H_2O and CO_2 fluxes at the floor of a boreal pine forest. *Tellus B*, **60**, 167-178.

Kutzbach L (2006) The exchange of energy, water and carbon dioxide between wet arctic tundra and the atmosphere at the Lena River Delta, Northern Siberia. *Reports on Polar and Marine Research,* **541**, Alfred-Wegener-Institut, Bremerhaven, Germany.

Kutzbach L, Schneider J, Sachs T *et al.* (2007) CO_2 flux determination by closed-chamber methods can be seriously biased by inappropriate application of linear regression. *Biogeosciences*, **4**, 1005-1025.

Kutzbach L, Wagner D, Pfeiffer EM (2004) Effect of microrelief and vegetation on methane emission from wet polygonal tundra, Lena Delta, Northern Siberia. *Biogeochemistry*, **69**, 341-362.

Kutzbach L, Wille C, Pfeiffer EM (2007) The exchange of carbon dioxide between wet arctic tundra and the atmosphere at the Lena River Delta, Northern Siberia. *Biogeosciences*, **4**, 869-890.

Liebner S, Wagner D (2007) Abundance, distribution and potential activity of methane oxidizing bacteria in permafrost soils from the Lena Delta, Siberia. *Environmental Microbiology*, **9**, 107-117.

Mastepanov M, Sigsgaard C, Dlugokencky EJ, Houweling S, Strom L, Tamstorf MP, Christensen TR (2008) Large tundra methane burst during onset of freezing. *Nature*, **456**, 628-630.

Morrissey LA, Zobel DB, Livingston GP (1993) Significance of stomatal control on methane release from Carex-dominated wetlands. *Chemosphere*, **26**, 339-355.

Nakano T, Kuniyoshi S, Fukuda M (2000) Temporal variation in methane emission from tundra wetlands in a permafrost area, northeastern Siberia. *Atmospheric Environment*, **34**, 1205-1213.

Reeburgh W, King J, Regli S, Kling G, Auerbach N, Walker D (1998) A CH_4 emission estimate for the Kuparuk River basin, Alaska. *Journal of Geophysical Research*, **103**, 29005-29013.

Riutta T, Laine J, Aurela M *et al.* (2007) Spatial variation in plant community functions regulates carbon gas dynamics in a boreal fen ecosystem. *Tellus B*, **59**, 838-852.

Sachs T, Wille C, Boike J, Kutzbach L (2008) Environmental controls on ecosystem-scale CH_4 emission from polygonal tundra in the Lena River Delta, Siberia. *Journal of Geophysical Research*, **113**, G00A03.

Schimel J (1995) Plant transport and methane production as controls on methane flux from arctic wet meadow tundra. *Biogeochemistry*, **28**, 183-200.

Schneider J, Grosse G, Wagner D (2009) Land cover classification of tundra environments in the Arctic Lena Delta based on Landsat 7 ETM+ data and its application for upscaling of methane emissions. *Remote Sensing of Environment*, **113**, 380-391.

643 Schuchard-Ficher C, Backhaus K, Humme U, Lohrberg W, Plinke W, Schreiner W (1982)
644 *Multivariate Analysemethoden. Eine anwendungsorientierte Einführung*. Springer,
645 Berlin, Heidelberg, New York.
646 Schwamborn G, Rachold V, Grigoriev MN (2002) Late Quaternary sedimentation history of
647 the Lena Delta. *Quaternary International*, **89**, 119-134.
648 Soil Survey Staff (1998) *Keys to Soil Taxonomy 8th Edition*. Pocahontas, Blacksburg,
649 Virginia, USA.
650 Spott O (2003) *Frostmusterbedingte Seen der Polygonalen Tundra und ihre Funktion als*
651 *Quellen atmospärischen Methans*. Unpublished Diploma Thesis, University of
652 Leipzig, Leipzig, Germany, 125 pp.
653 von Storch J (2004) On statistical dissipation in GCM-climate. *Climate Dynamics*, **23**, 1-15.
654 Suyker A, Verma S, Clement R, Billesbach D (1996) Methane flux in a boreal fen: Season-
655 long measurement by eddy correlation. *Journal of Geophysical Research*, **101**, 28637-
656 28647.
657 Wagner D, Kobabe S, Pfeiffer EM, Hubberten H (2003) Microbial controls on methane fluxes
658 from a polygonal tundra of the Lena Delta, Siberia. *Permafrost and Periglacial*
659 *Processes*, **14**, 173-185.
660 Walter KM, Zimov SA, Chanton JP, Verbyla D, Chapin FS (2006) Methane bubbling from
661 Siberian thaw lakes as a positive feedback to climate warming. *Nature*, **443**, 71-75.
662 Wanninkhof R, McGillis WR (1999) A Cubic Relationship Between Air-Sea CO_2 Exchange
663 and Wind Speed. *Geophysical Research Letters.*, **26**, 1889-1892.
664 Whalen SC, Reeburgh WS (1996) Moisture and temperature sensitivity of CH_4 oxidation in
665 boreal soils. *Soil Biology and Biochemistry*, **28**, 1271-1281.
666 Whalen SC, Reeburgh WS (1990) A methane flux transect along the trans-Alaska pipeline
667 haul road. *Tellus B*, **42**, 237-249.

668 Whalen SC, Reeburgh WS (1988) Methane Flux Time Series for Tundra Environments. *Global Biogeochemical Cycles*, **2**, 399-409.

670 Whiting G, Chanton J (1993) Primary Production Control of Methane Emission from Wetlands. *Nature*, **364**, 794-795.

672 Wickland KP, Striegl RG, Neff JC, Sachs T (2006) Effects of permafrost melting on CO_2 and CH_4 exchange of a poorly drained black spruce lowland. *Journal of Geophysical Research*, **111**, G02011.

675 Wille C, Kutzbach L, Sachs T, Wagner D, Pfeiffer EM (2008) Methane emission from Siberian arctic polygonal tundra: eddy covariance measurements and modeling. *Global Change Biology*, **14**, 1395-1408.

678 Zona D, Oechel WC (2008) Continuous measurements of methane fluxes by eddy covariance in the Arctic: Results of a large-scale manipulation of water status at Barrow, Alaska. *Geophysical Research Abstracts*, **10**, EGU2008-A-10980.

Table 1: Species and percent coverage for each 50x50cm closed chamber plot (data provided by Merten Minke, 5 July 2006).

	Polygon 1: wet low-center; early degradation			Polygon 2: well-drained high-center; final stage of degradation			Polygon 3: wet low center; advanced degradation			Polygon 4: inundated low-center; no visible degradation			Polygon 5: polygon rim; no standing water		
Species / plot	1	2	3	1	2	3	1	2	3	1	2	3	1	2	3
Vascular plants															
Astragalus frigidus	-	-	-	-	-	-	-	-	-	-	-	-	0.5	1	1
Carex chordorrhiza	10	8	3	-	-	-	30	10	5	7	7	10	-	-	-
Carex concolor	0.1	1	0.1	2	1	0.5	3	5	10	3	3	3	3	3	5
Comarum palustre	1	1	2	-	-	-	2	5	5	3	3	2	-	-	-
Draba pilosa	-	-	-	-	-	-	-	-	-	-	-	-	-	-	0.1
Dryas punctata	-	-	-	-	0.5	1	-	-	-	-	-	-	1	-	-
Equisetum arvense	-	-	-	-	-	0.1	-	-	-	-	-	-	-	-	-
Hierochloe pauciflora	-	-	-	-	-	0.1	-	-	-	-	-	-	-	-	-
Lagotis	-	-	-	0.1	-	-	-	-	-	-	-	-	-	-	-
Parrya nudicaulis	-	-	-	-	-	-	-	-	-	-	-	-	0.1	-	-
Poa arctica	-	-	-	0.1	0.1	-	-	-	-	-	-	-	-	0.1	-
Polygonum viviparum	-	-	-	0.1	0.1	0.1	-	-	-	-	-	-	-	-	-
Pyrola rotundifolia	-	-	-	-	-	-	-	-	-	-	-	-	0.1	0.5	2
Salix glauca or S.reptans	-	-	-	1	0.5	0.1	-	-	-	-	-	-	-	-	-
Saussurea sp.	-	-	-	-	-	-	-	-	-	-	-	-	0.1	0.1	0.1
Mosses															
Aulacomnium turgidum	0.5	-	-	0.5	0.5	5	10	10	5	-	-	-	1	-	0.5
Calliergon giganteum	0.1	0.1	0.1	-	-	-	0.1	0.1	0.1	0.1	0.1	-	-	-	-
Drepanocladus cf. vernicosus	-	-	0.1	-	-	-	50*	-	-	-	-	-	-	-	-
Drepanocladus revolvens	-	-	-	-	-	-	40*	85*	95*	-	-	-	-	-	-
Hylocomium splendens	-	-	-	90	80	85	-	-	-	-	-	-	50	30	99
Meesia triquetra	0.5	0.1	0.5	-	-	-	1	3	0.1	-	-	-	-	-	-
Polytrichum cf. alpinum	-	-	-	-	-	-	-	-	-	-	-	-	5	2	0.1
Rhytidium rugosum	-	-	-	-	-	-	-	-	-	-	-	-	40	60	2
Scorpidium scorpioides	99	100	99	-	-	-	-	-	-	100	100	100	-	-	-
Tomentypnum nitens	-	-	-	10	20	5	-	-	-	-	-	-	-	-	-
Lichens															
Cetraria laevigata	-	-	-	-	-	-	-	-	-	-	-	-	0.5	0.1	0.5
Dactylina arctica	-	-	-	-	-	-	-	-	-	-	-	-	-	0.1	0.5
Peltigera sp.	-	-	-	1	-	5	-	-	-	-	-	-	0.5	1	1
Stereocaulon sp.	-	-	-	-	-	-	-	-	-	-	-	-	-	-	0.1

Table 2: Seasonally averaged, maximum, minimum, and modeled cumulative methane fluxes from the five different micro-sites.

polygon	average flux ($mg\ m^{-2}\ d^{-1}$)	maximum flux ($mg\ m^{-2}\ d^{-1}$)	minimum flux ($mg\ m^{-2}\ d^{-1}$)	modeled cum. flux ($g\ m^{-2}$)
1	77.9	278.4 ± 307.2	9.3 ± 15.8	3.95 ± 0.01
2	10.5	39.1 ± 55.3	-1.9 ± 4.1	0.72 ± 0.08
3	100.0	363.8 ± 259.8	8.8 ± 7.3	4.93 ± 0.01
4	80.8	161.6 ± 118.1	1.8 ± 3.3	4.26 ± 0.01
5	4.9	28.2 ± 36.9	–3.6 ± 20.3	0.34 ± 0.05

Table 3: Results of the error-weighted linear regressions shown in Fig. 7 given by $F_{CH4} = a + bx$, where x is the surface temperature as calculated by the Stefan-Boltzmann equation and F_{CH4} is the modeled methane flux.

Polygon	Parameter	Value	Error	*t*-value	*p*>|*t*|	[a]LCI	[b]UCI	*R*	[c]R^2_{adj}	[d]*RMSE* (*mg* m^{-2} d^{-1})
1	*a* (*mg* m^{-2} d^{-1})	23.2	4.3	5.381	<0.0001	14.435	31.895	0.82	0.66	1.16
	b (°C^{-1})	5.1	0.5	10.015	<0.0001	4.097	6.178			
3	*a* (*mg* m^{-2} d^{-1})	21.4	3.4	6.386	<0.0001	14.625	28.219	0.85	0.72	1.80
	b (°C^{-1})	7.5	0.4	17.777	<0.0001	6.688	8.409			
4	*a* (*mg* m^{-2} d^{-1})	22.3	2.3	9.762	<0.0001	17.627	26.883	0.91	0.83	1.33
	b (°C^{-1})	6.0	0.3	17.769	<0.0001	5.277	6.638			

[a]LCI is the lower confidence interval, [b]UCI is the upper confidence level, [c]R^2_{adj} is the adjusted R^2 taking into consideration the number of explanatory variables and [d]*RMSE* is the root mean squared error.

Table 4: Surface classes and average August methane emissions in the eddy covariance footprint. The area-weighted chamber fluxes (total emission) add up to the flux measured by eddy covariance. In a scenario with precipitation, lower temperatures, and higher wind speed, fluxes from very wet soils are assumed to be reduced by 20%, while fluxes from drier or moist soils are conservatively assumed to increase three-fold (they increased up to five-fold). The total ecosystem flux increases despite weather conditions usually associated with lower emissions.

Surface class	**Coverage (%)**	**CH_4 flux (mg m^{-2} d^{-1})**	**Total flux (mg m^{-2} d^{-1})**	**Flux scenario (mg m^{-2} d^{-1})**	**Source of emission rate**
Very wet soils (inundated low-center polygons)	10	94.1	9.4	7.5	Polygon 1, 3, 4 (this study)
Drier or moderately moist soils (high-center polygons and rims)	62	7.7	4.8	14.3	Polygon 2 and 5 (this study)
Open water without ebullition (ponds, lakes, cracks)	14	2.4	0.3	0.3	Spott (2003)
Additional flux by ebullition		0 to 30	0 to 4.2	0 to 4.2	
Overgrown water (small ponds, cracks, shores)	14	44.9	6.3	6.3	Spott (2003)
Eddy covariance footprint (without / with ebullition)	100	20.6	20.8 20.8 to 25.0	28.4 28.4 to 32.6	Sachs *et al.* (2008)

Figure 1: (left) Location of the investigation area and vegetation zones in the Arctic (modified after work by UNEP/GRID-Arendal (1996)). **(right)** Location of the study site Samoylov Island in the Lena River Delta (marked by the square (satellite image: Landsat 7 Enhanced Thematic Mapper (on Nimbus 6)+ GeoCover 2000, NASA (Landsat imagery courtesy of NASA Goddard Space Flight Center and U.S. Geological Survey) (Map by G. Grosse, AWI Potsdam))).

Figure 2: Aerial images of the study site. **(left)** Mosaic of aerial images of Samoylov Island taken in August 2007 (Boike *et al.* 2008a). **(right)** The central part of Samoylov Island in August 2007. The asterisk marks the position of the micrometeorological tower. The inset shows the closed chamber study area in direct proximity to the tower. The numbers refer to the micro-sites 1-5.

Figure 3: Schematic overview of the dominant micro-sites. From left to right: thermokarst crack (not explicitly covered in this study), high-center polygon (Polygon 2) surrounded by crack or troughs, wet low-center polygon (Polygon 1, 3, and 4), polygon rim (Polygon 5), and pond/lake (not explicitly covered). The dense diagonal hatching from bottom left to top right marks the permafrost. The wider diagonal hatching in the opposite direction shows mineral soil layers within the seasonally thawed active layer and the denser diagonal hatching on the top denotes the organic layer. The water level is represented by the blue line.

Figure 4: Examples for non-linear evolution of CH_4 concentration in the closed chamber headspace for different micro-sites and dates. The exponential fits of the form $c\mathrm{CH_4} = \beta_1 + \beta_2 \exp(\beta_3\, t)$ are also given for each concentration curve.

Figure 5: Meteorological conditions during the measurements campaign. **(a)** hourly wind speed and atmospheric pressure measured at the eddy covariance tower. **(b)** daily precipitation measured at the long-term climate station 700 m south of the closed chamber site, hourly air temperature in 2 m height measured at the eddy covariance tower, and surface temperature calculated from outgoing long-wave radiation using the Stefan-Boltzmann equation.

Figure 6: (left) closed chamber methane fluxes from micro-sites 1–5 (a-e). Black error bars denote the averaged standard error of the six replicate measurements per micro-site. Grey error bars denote the standard deviation of the replicate measurements within a micro-site, providing information about the spatial variability. The grey line shows the modeled fluxes for the wet low center polygons 1 (a), 3 (c), and 4 (d) using the functions shown in Fig. 7 and Table 3. **(right)** water table, active layer depth, and soil temperatures in 10, 20, and where applicable 30 cm depth for each of the micro-sites.

Figure 7: Standard-error weighted linear regression models with surface temperature as the best predictor for methane fluxes from polygon 1 ($F_{CH4} = 23.2 + 5.1 \cdot x$), polygon 3 ($F_{CH4} = 21.4 + 7.5 \cdot x$), and polygon 4 ($F_{CH4} = 22.3 + 6.0 \cdot x$).

Figure 8: Comparison of closed chamber (left axes) vs. eddy covariance (right axes) methane fluxes and the dominant controls. **(a)** closed chamber methane fluxes from micro-sites 2 (high center polygon) and 5 (polygon rim) are shown on the left y-axis on the same scale as the eddy covariance flux on the right y-axis. The main predictor of eddy covariance methane flux is near-surface turbulence (i.e. friction velocity u_*.), which was exaggerated 50x to fit on the same scale. **(b)** closed chamber methane fluxes from wet polygon center micro-sites 1, 3, and

4 are shown on the left y-axis and eddy covariance methane flux is shown on the right y-axis along with surface temperature as the only significant predictor of the chamber-based fluxes. Note the different scales.

Figure 9: Surface classification of a high-resolution aerial image of the study site. The white asterisk in the center of the image marks the position of the eddy covariance tower. Open water covers about 14% of the surface, wet areas (inundated polygon centers and overgrown water, separated in table 4) cover 24% of the surface, and moist/dry areas (high-center polygons and rims, combined in table 4) cover 62% of the surface.

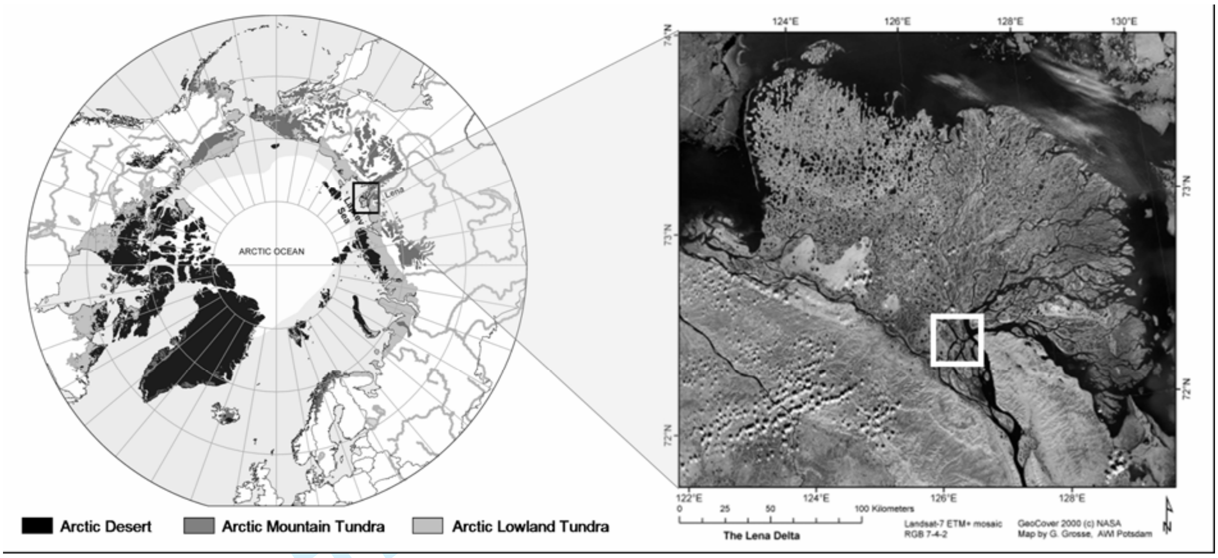
ARCTIC OCEAN
Lena
124°E
126°E
128°E
130°E
74°N
73°N
72°N
122°E
0 25 50 100 Kilometers
The Lena Delta
Landsat-7 ETM+ mosaic
RGB 7-4-2
GeoCover 2000 (c) NASA
Map by G. Grosse, AWI Potsdam
Arctic Desert
Arctic Mountain Tundra
Arctic Lowland Tundra

759

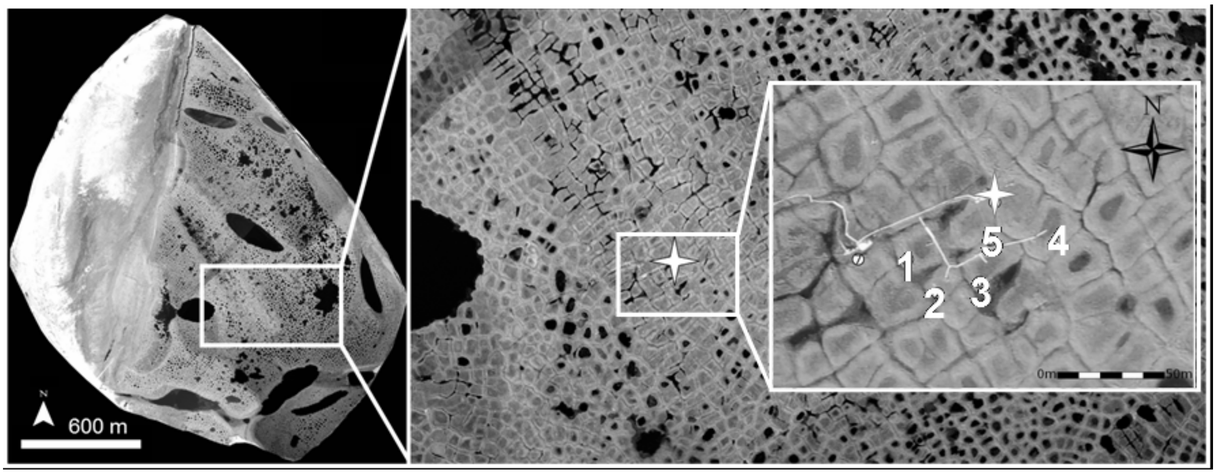

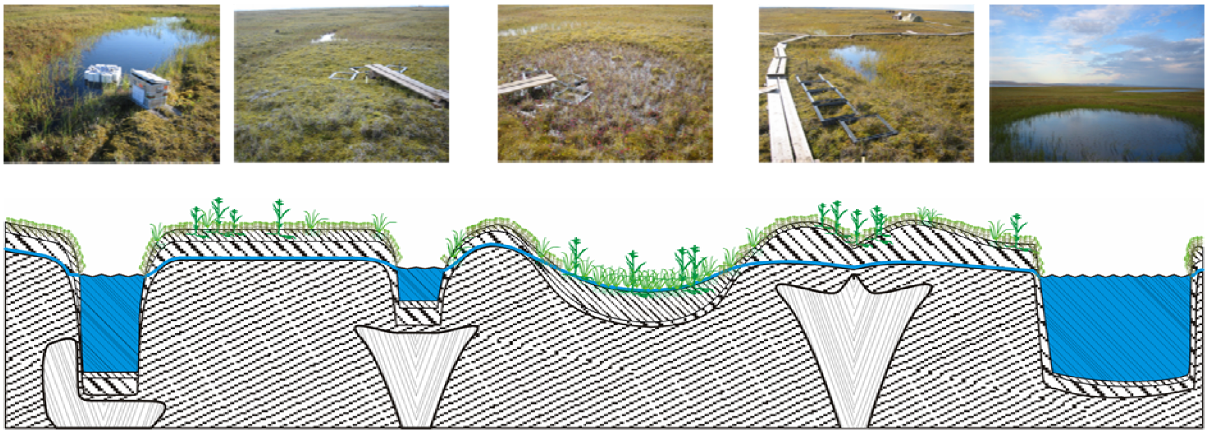

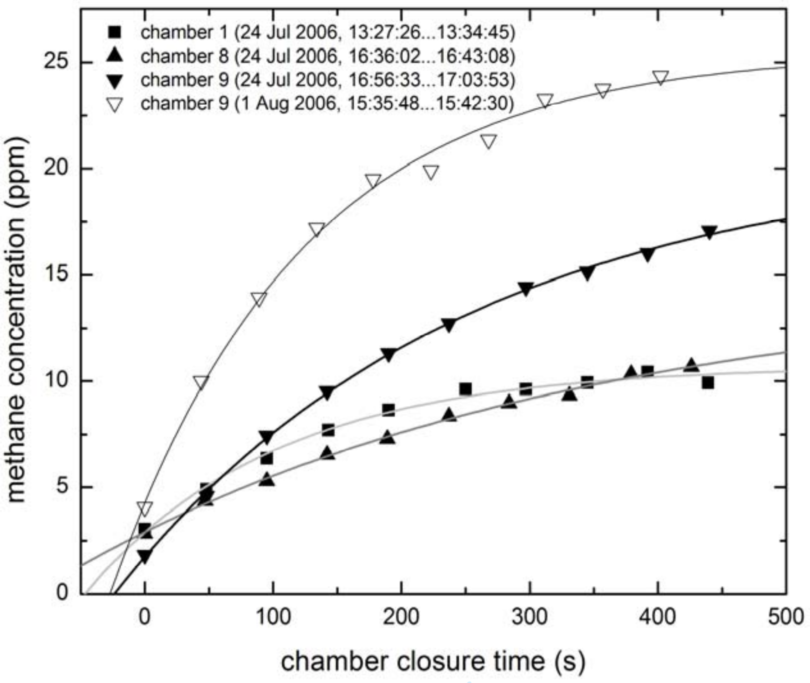
chamber 1 (24 Jul 2006, 13:27:26...13:34:45)
chamber 8 (24 Jul 2006, 16:36:02...16:43:08)
chamber 9 (24 Jul 2006, 16:56:33...17:03:53)
chamber 9 (1 Aug 2006, 15:35:48...15:42:30)
methane concentration (ppm)
0
5
10
15
20
25
0
100
200
300
400
500
chamber closure time (s)

761

762

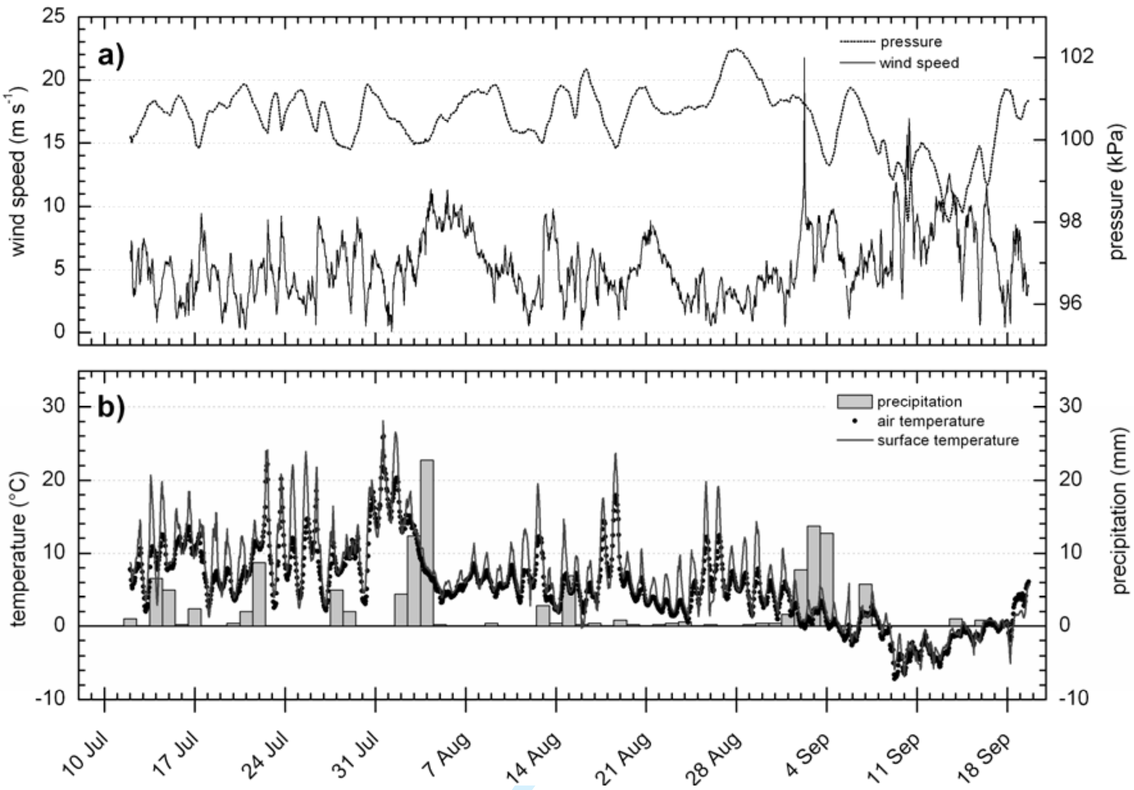
a)
pressure
wind speed
wind speed (m s-1)
pressure (kPa)
25
20
15
10
5
0
102
100
98
96
b)
precipitation
air temperature
surface temperature
temperature (°C)
precipitation (mm)
30
20
10
0
-10
10 Jul
17 Jul
24 Jul
31 Jul
7 Aug
14 Aug
21 Aug
28 Aug
4 Sep
11 Sep
18 Sep

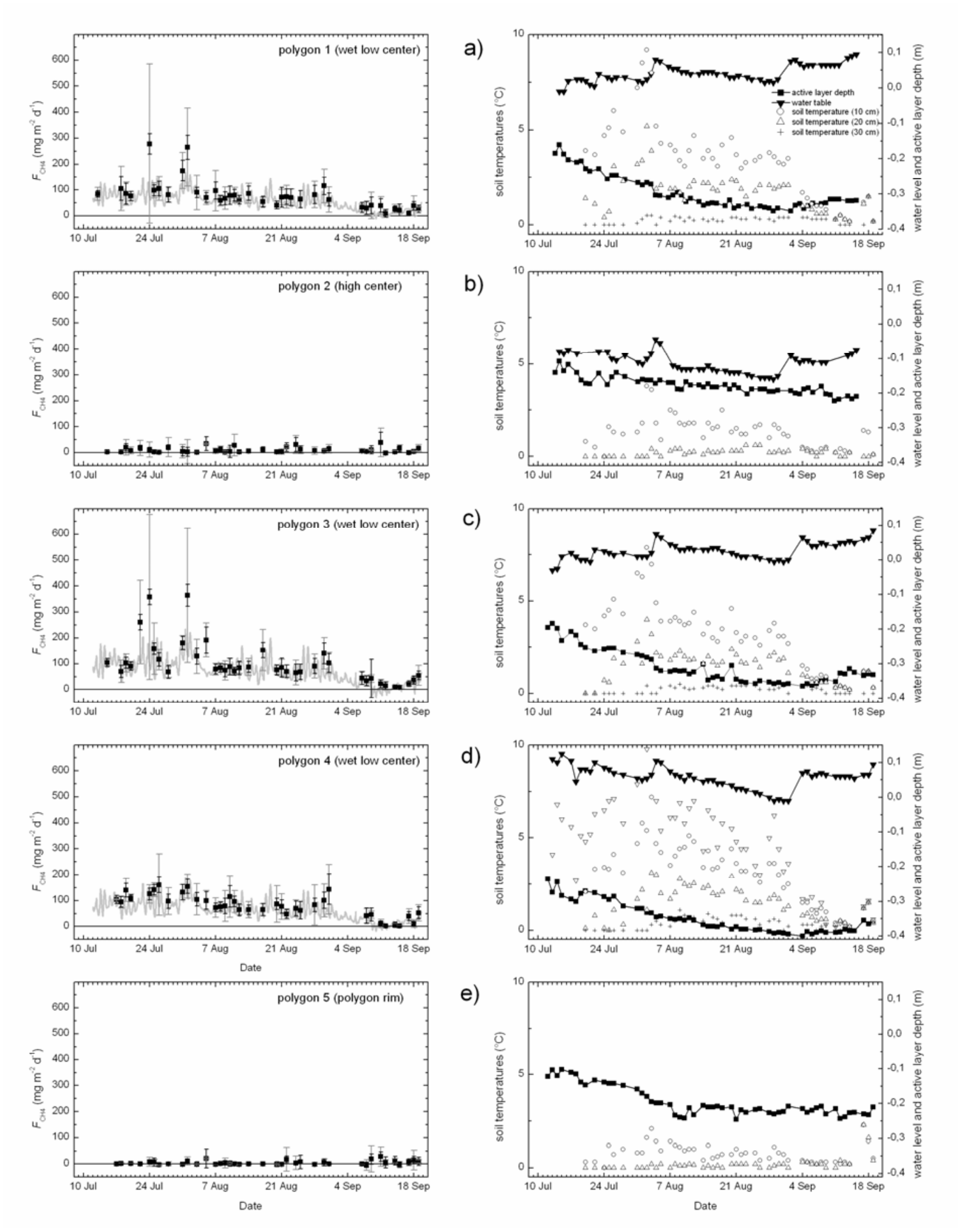
polygon 1 (wet low center)
polygon 2 (high center)
polygon 3 (wet low center)
polygon 4 (wet low center)
polygon 5 (polygon rim)
a)
b)
c)
d)
e)
F_CH4 (mg m-2 d-1)
soil temperatures (°C)
water level and active layer depth (m)
active layer depth
water table
soil temperature (10 cm)
soil temperature (20 cm)
soil temperature (30 cm)
10 Jul
24 Jul
7 Aug
21 Aug
4 Sep
18 Sep
Date

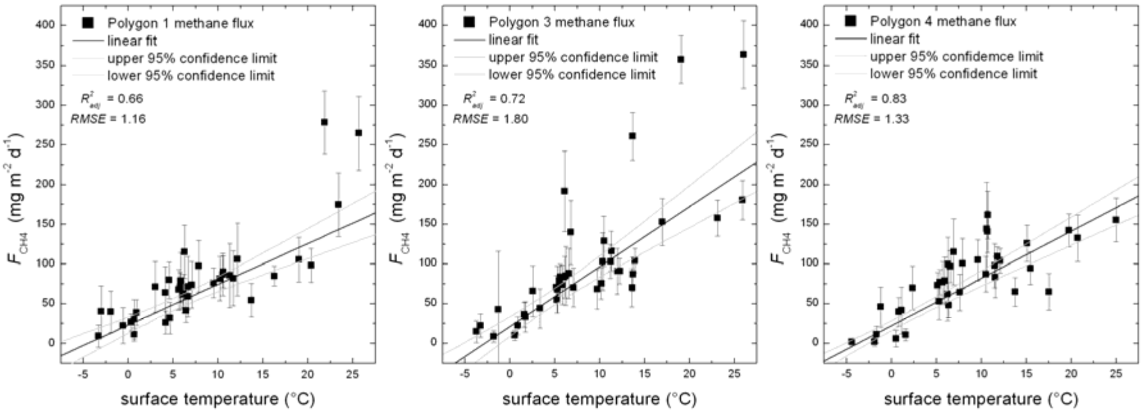
Polygon 1 methane flux
linear fit
upper 95% confidence limit
lower 95% confidence limit
R^2_{adj} = 0.66
RMSE = 1.16
Polygon 3 methane flux
linear fit
upper 95% confidence limit
lower 95% confidence limit
R^2_{adj} = 0.72
RMSE = 1.80
Polygon 4 methane flux
linear fit
upper 95% confidemce limit
lower 95% confidence limit
R^2_{adj} = 0.83
RMSE = 1.33
F_{CH4} (mg m^{-2} d^{-1})
surface temperature (°C)

765 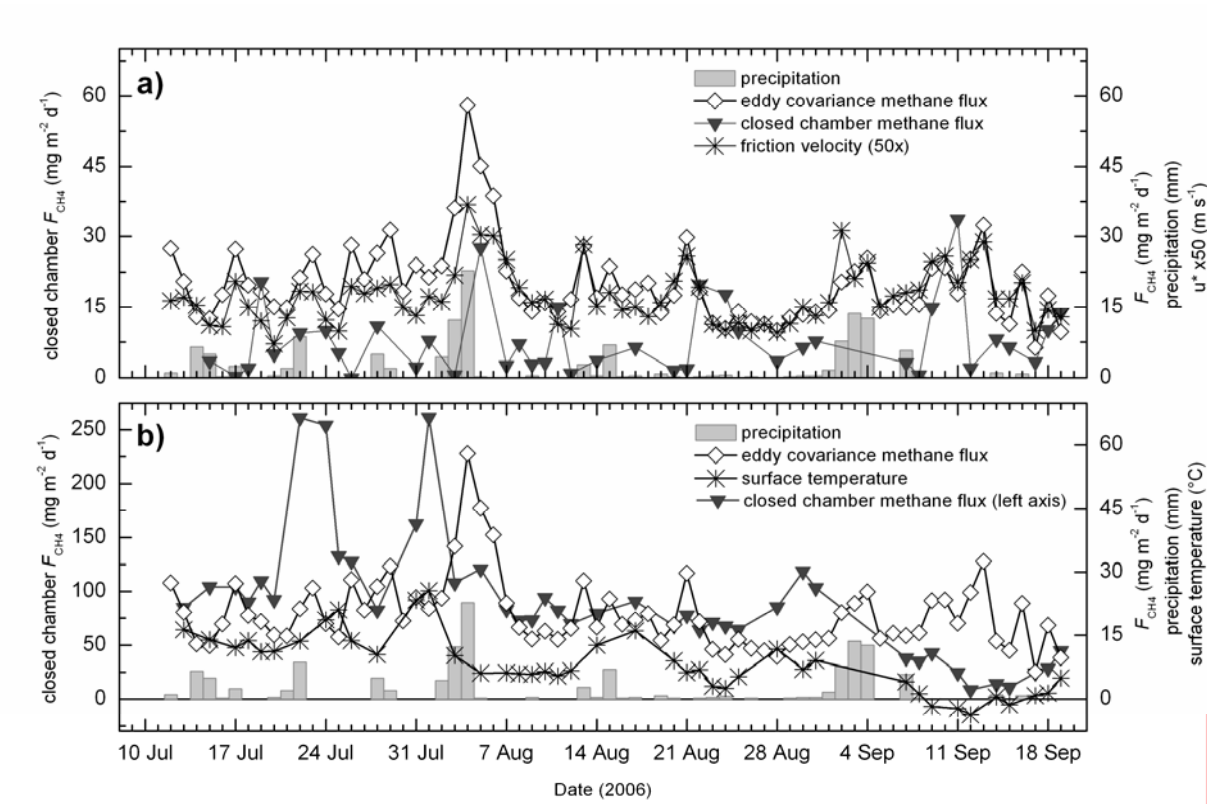
a)
precipitation
eddy covariance methane flux
closed chamber methane flux
friction velocity (50x)
closed chamber F_{CH4} (mg m^{-2} d^{-1})
F_{CH4} (mg m^{-2} d^{-1})
precipitation (mm)
u* x50 (m s^{-1})
b)
precipitation
eddy covariance methane flux
surface temperature
closed chamber methane flux (left axis)
closed chamber F_{CH4} (mg m^{-2} d^{-1})
F_{CH4} (mg m^{-2} d^{-1})
precipitation (mm)
surface temperature (°C)
10 Jul
17 Jul
24 Jul
31 Jul
7 Aug
14 Aug
21 Aug
28 Aug
4 Sep
11 Sep
18 Sep
Date (2006)

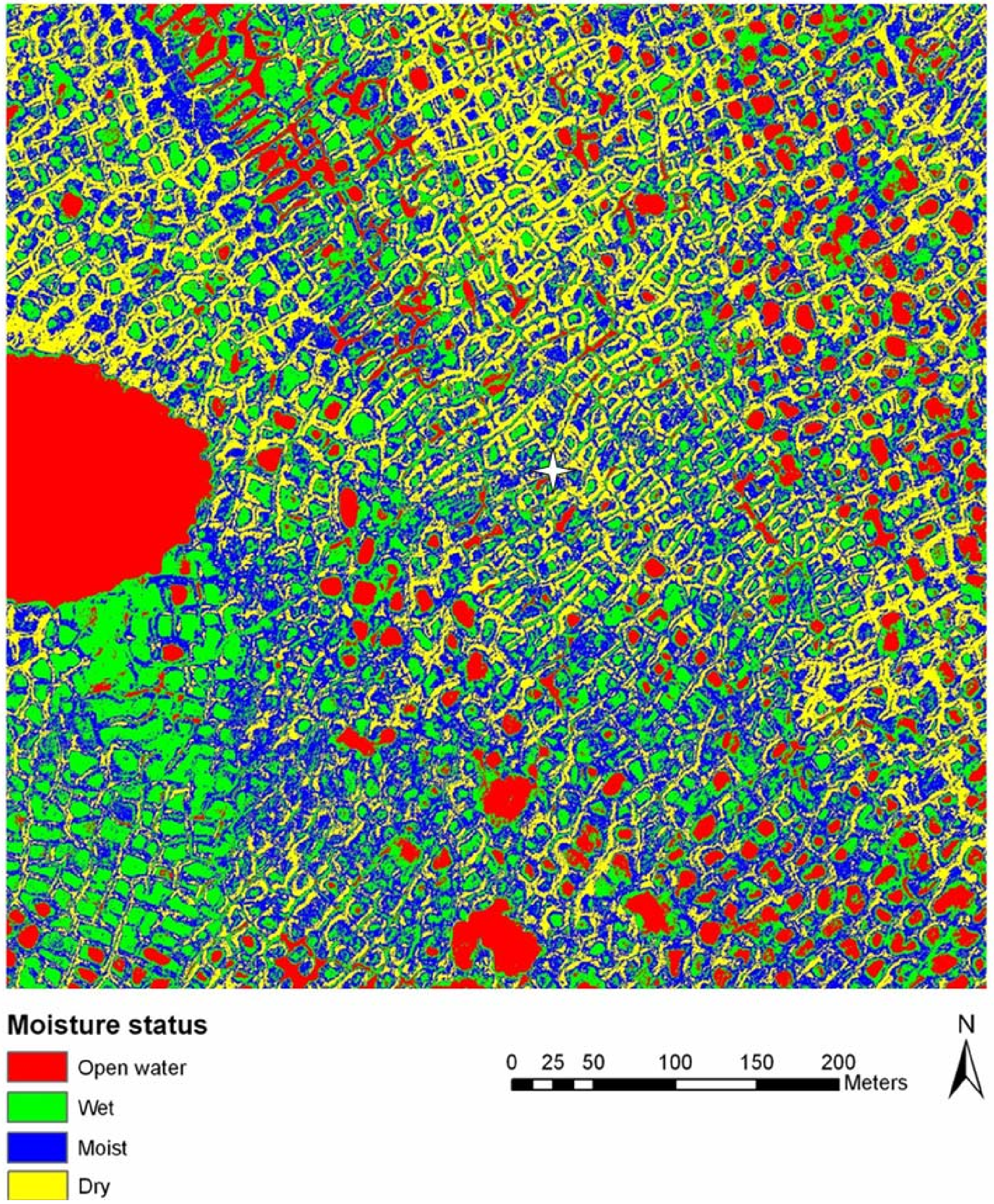
Moisture status
Open water
Wet
Moist
Dry
0 25 50 100 150 200
Meters
N

766

GFZ Helmholtz Centre POTSDAM

HELMHOLTZ CENTRE POTSDAM
GFZ GERMAN RESEARCH CENTRE FOR GEOSCIENCES

GFZ · Postfach 60 07 51 · 14407 Potsdam · Germany

Dr. Eric A. Davidson
Subject Editor

Global Change Biology

Dr. Torsten Sachs
Section 4.2

torsten.sachs@gfz-potsdam.de

Telefon: +49 (0)331 288-1429

Telefax: +49 (0)331 288-1474

Revised Manuscript 09-0144

Potsdam, 09.02.2010

Dear Dr. Davidson,

Enclosed, please find our revised manuscript entitled „Environmental controls on CH4 emission from polygonal tundra on the micro-site scale in the Lena River Delta, Siberia".

We thank you and the reviewers for the helpful comments and have incorporated all suggestions where possible.

Unfortunately, some points may not have been possible to change to your satisfaction. We are absolutely aware that the lack of contemporary data from the water bodies is a weakness and had the necessary human and logistical resources been available or another expedition been possible to collect those data, I certainly would have done so. Unfortunately, that lack of data also affects our ability to investigate the scaling problem on shorter time scales than just a monthly average, which several reviewers had asked for. Considering the short-term variability of weather conditions, we feel it is inappropriate to use data from two different years to investigate daily or weekly periods and feel more comfortable with the monthly average.

We shortened the manuscript substantially in the sections suggested by you and the reviewers and hopefully succeeded in making it more to the point.

Sincerely,

Torsten Sachs

HELMHOLTZ ASSOCIATION

Reply to Editor's and Reviewers' Comments:

Editor's comments:

The reviewer is also concerned about uncertainty in classification of areas of cover types. The reviewer focuses on the Boike et al 2009 publication, but I was also confused on pages 25-26 about Schneider et al. 2009 and the personal communication of Muster. As I understand it, Schneider et al. studied an area further south, but do the areal estimates in Table 3 come from Schneider and do they apply to your specific area? Were they modified by Muster to apply to your area? Some clarity is needed here. If Schneider et al provide sufficient error analysis of their classification, a brief statement and citation should suffice to address the reviewer's concerns. Otherwise, some additional analysis might be needed.

→ The correct Boike et al. 2008 reference was missing from the reference list and describes the acquisition of the underlying aerial imagery that was used for Fig. 2 and for the classification. Schneider et al. 2009 classified the area around our tower from (older) aerial images. The methane emissions Schneider et al. used for upscaling were from a closed chamber site about 700 m south of our site and outside of the image area used for the high-res surface classification. Our own classification is based on new imagery and covers a slightly larger area around the EC tower, and therefore our area fractions differ slightly from Schneider et al. The estimates in Table 3 (now Table 4) come from our own classification, and based on our knowledge of the site and the methane emissions we merged the classes "moist" and "dry" into one class that represents high center polygons and polygon rims, which show very similar methane emissions. Similarly, we separated the "wet" class into very wet polygon centers and vegetated water areas ("overgrown water"), because these two differ in their typical methane source strength. The area estimates in this case are based on Schneider et al.. While the classification itself was an unsupervised k-means classification in ENVI 4.6, we then thoroughly checked the result based on the underlying high-resolution photographs and our knowledge of the site to correct any possible misclassifications. Schneider et al. describe their accuracy assessment for the entire delta on page 382 of Schneider et al. 2009, but this refers to the Landsat based classification and not to the near-surface aerial images.

Here are my own suggestions:

1. Section 5.2 should be shortened considerably. It is not necessary to give mean, range, and standard error in the text for each microsite. Nor is it necessary to describe how fluxes changed seasonally for each microsite. Nearly all of that information is given in Figure 6 and you could add a table if you think that it necessary. You need only comment in the text on highlights from tables and figures to which you wish to draw the reader's attention or which may not be obvious. For example, mentioning snow fall and ice cover may be appropriate, unless that can be shown with an arrow or other symbol in the figure. The figure is busy and complex, so some emphasis on its most important points are warranted, but this section comments on everything, which doesn't really help the reader much. The reader wants you to guide him/her through the most important findings as quickly as possible.

→ We have shortened section 5.2 by almost 65% and included a table (table 2) to summarize mean, max, min, and cumulative modeled flux for the five microsites.

2. Line 363: What is the detection limit of the instrument? Actually, "high" and "low" are relative terms, and in this case you refer to fluxes relative to the sensitivity of the instrument.

→ We deleted the reference to the detection limit during rewriting of the entire section. The important point is that low concentrations and noisy data often led to exclusion of the measurements during flux calculation. The detection limit as given by the manufacturer was 0.4 ppm for the optical filter we used.

3. Lines 438-456: This is another section that could be cut substantially, if not completely. This is very speculative and convoluted. You will lose most readers here. Are these points really important? In fact, I suggest you go over all of section 6.1 to see if you can make it more to the point.
→ We shortened section 6.1 by a third and hopefully made it more to the point.

4. Your biggest challenge (and opportunity) is to improve section 6.2 and Table 3. This is the part that the reviewers and I find novel and that could quality the manuscript for acceptance in this journal, but it is not well enough developed. You have demonstrated in Table 3 that bottom-up scaling with mean flux values measured in August agree roughly with eddy covariance mean flux estimates for the same period. Did you "cherry-pick" the one month where this worked? Can you do the same for other months? Was there a period when it didn't work out so well? If so, why might that be? Could you use the temperature function for wet sites and the correlation with friction velocity for the dry sites to estimate daily or weekly fluxes by the bottom-up approach, and then compare those estimates with eddy covariance measurements across most or all of the study period?
→ No, we did not cherry-pick the month where the scaling worked. We did, however, cherry-pick the only month, where data from all micro-sites where available for an entire month. Because we do not have own data from water bodies, we decided it would be unacceptable to investigate the scaling issue on a daily time scale and chose the monthly averages instead. We considered this to be the most acceptable option given the fact that we had to mix data from 2002 and 2006. However, in preparing the revised version we did also check weekly and biweekly periods. For the weekly periods, eddy covariance and scaled chamber fluxes were within ± 10% of each throughout July. The first week of August, which in 2006 was characterized by a strong storm lasting several days, and the last week of August were the periods with the largest differences between eddy covariance and scaled chamber fluxes. For bi-weekly periods accordingly, the first two weeks in July and the two weeks in the middle of August showed the best agreement (within 10% of each other).
However, due to the unfortunate data situation we would prefer to keep the monthly average to demonstrate the scaling. Monthly averaged water body methane emissions are more likely to be comparable between different years than those from shorter periods as changing weather conditions may average out. In addition, for short time periods, a more detailed footprint analysis would be necessary. On a monthly time scale, we consider it reasonable to assume that differences in footprint composition average out as well.
In addition, the main point here is not to show in absolute detail whether scaled chamber measurements and eddy covariance measurements match with regard to total fluxes. One of the unique features of this site compared to other eddy covariance and closed chamber study sites is the polygonal pattern and the associated strong differences not just in the methane flux itself but also its dominant drivers. In environments such as this, the low emitting micro-sites can easily be dismissed as not relevant to the ecosystem flux. This study, however, shows that the dominant drivers of methane emission are not necessarily the same for the different micro-sites and spatial scales and these differences between "dry" sites vs. wet sites may easily cause the low flux micro-sites to change the ecosystem flux towards (unexpected) increased emissions during weather conditions typically associated with decreased methane emissions (i.e. low temperatures, rain, strong winds). We extended table 4 to include this thought experiment.

5. lines 586-587: I don't understand what was personally communicated by Petrescu and Zhang. I would avoid using personal communications if possible. If they really contributed to your intellectual interpretation of the data, they should join as coauthors. If they provided a key piece of data that is unpublished, what they provided should be clearly identified. The same goes for Muster.
→ Petrescu et al. used our data for comparison with model results from the PEATLAND-VU model and Zhang et al. use our data for comparison with results from the integrated wetland-

DNDC and NEST model. In both cases, the models were not able to reproduce our eddy covariance data but compared more favorably with the closed chamber data. That information was just a personally communicated by-product of modeling efforts that will be thoroughly described and published elsewhere. We don't think every single bit of exchanged information automatically warrants co-authorship and thus don't see why personal communication should be avoided. Nevertheless, we changed the text and hopefully it is more understandable now.

6. There are several points about the figures. I hope you are aware of the color figure charges of the journal, which would be substantial for your four color figures.
→ Thanks for the hint!

Unfortunately, two of the black-and-white figures (6 and 8) are difficult to read and might be improved with color, although there may be other ways to improve them as well. The legend is too small for Figure 6. The symbols should also be bolder and/or bigger. The eddy covariance symbols and line are very difficult to see in Figure 8.
→ We increased the legend and symbol sizes.

I also didn't understand why eddy covariance is presented in both panels and which scale (upper or lower panel) is the correct one for the eddy covariance fluxes. I presume it is the top panel, but it is confusing that the eddy covariance values are also shown in the lower panel without the correct scale on the Y axis – or am I misunderstanding something?
→ We presented the eddy covariance fluxes in both panels for easier comparison to the chamber fluxes. We tried to make the axis labeling more coherent: closed chamber methane fluxes are now on the left y-axis on both panels, and eddy covariance methane fluxes are on the right y-axis.

The figure 6 caption is confusing. I don't understand what "the mean of the standard error of each or the six replicate measurements per microsite" means. I assume that "or" should be "of", but even with that typo corrected, I still don't understand it. Are these "replicates" in time? I presume that the "modeled fluxes" are based on the functions shown in Figure 7 and Table 2, but that is not clear. The Table 2 caption further confuses matters, because x and y are not defined. Does Table 2 report the fitted functions shown in Fig. 7? If so, these captions should cross-reference each other.
→ There are up to six measurements per polygon, each of which has an associated standard error. The black error bars are the averaged standard errors (now one bar per polygon per day). The grey error bars are the standard deviation of those up to six measurements per polygon. We corrected the table caption and cross-referenced the table and figure captions.

Reviewer(s)' Comments to Author:

Reviewer: 3

Given the spatial importance of the water bodies (28% coverage) I am perplexed as to why the authors relied on 2003 data from another researcher at the site, rather than contemporary measurements within THIS study. This lack of contemporary information is a real pity, as is the issue of near-surface turbulence.

→ We (and especially the first author) absolutely agree, that this is a pity. However, manpower simply did not allow for any meaningful additional measurement campaign focusing on the water bodies in 2006, and while I fought hard for such a campaign in 2007 it was unfortunately not approved by the department head. Without that approval and the massive financial and logistical support that comes with it, it is impossible to even get to the site, not to mention measure anything, and while we agree that this is a weakness of the study, there is absolutely nothing we can do about it. It still is the only site we know about in the entire Siberian Arctic where closed chambers and a tower were operated simultaneously and for a comparably long period of time.

P10. line 195 –"…..various depths" – which exactly?

→ 1 cm, 5 cm, 10 cm, 20 cm, 30 cm, and 40 cm depth in the polygon center, as well as in 5 cm depth intervals at a polygon rim.

P11. line 220- please provide more information to substantiate your cut-off of 0.3 ppm residual standard deviation.

→ Often, r^2 or R^2 are used as filter criteria for measurement performance and thresholds are set at 0.9 or 0.95. However, we consider these not usable as filter criteria because they arbitrarily discriminate against lower fluxes: r^2 and R^2 values increase with constant unexplained variance and increasing total variance which is inherently higher for greater fluxes. Thus, we consider the standard deviation of the residuals to be a better filter criterion. In order to be able to present an understandable and reproducible criterion (as opposed to just visually/subjectively determining which curves to accept and which to discard), the 0.3 ppm cut-off was chosen after checking residual standard deviation against the initial slope of the exponential regression function in addition to visually checking each curve.

Pages 15-18 – can this not be shortened considerably? It is all rather long-winded and a summary table might help this.

→ We have shortened section 5.2 by almost 65% and included a table (table 2) to summarize mean, max, min, and cumulative modeled flux for the five microsites.

P22. line 471. I am surprised that you rely upon the data of Spott (2003). Why did you not make some contemporary open water measurements during the campaign you report?

→ See above.

Figure 6. Annotate the figures a to e with reminder of which micro-sites they represent. Similarly, add this detail to the figure legend.

→ Done.

Figure 7. Legend: provide equations of the regression fits.

→ Done.

Fig. 8 - this figure does not make as much of the comparison it purports to show, as it could. I urge the authors to consider this point.
→ This is a bit unspecific. We changed figure 8 / the figure caption as suggested by the editor.

Fig. 8 (and earlier figs where appropriate). Please use (a), (b), (c) etc for the sub-figures in your composite figure rather than (top) and (bottom) for the sake of clarity (and consistency!).
→ Done.

Figure 8. legend does not require a discussion of the data within it – remove.
→ Done.

Check chemical symbols throughout, but especially in reference list – sub- and superscripts are not always accurate! E.g CH4 not CH4.
→ Corrected, thank you!

Reviewer: 4

As one of few Arctic flux sites, how representative is this delta site in comparison to other polygon tundra areas in Siberia?

→ We consider wet polygonal tundra to be more or less inherently fairly representative for any other wet polygonal tundra site, because in addition to the generally required presence of permafrost and low/rapidly falling winter temperatures, certain environmental conditions favor its development. For example, annual precipitation should be low because a thick insulating snow cover could prevent soil cooling and frost cracking. On the other hand, in order to form and support the water saturated low center polygons the area should be flat and sufficiently wet with no or very limited drainage. Climate and precipitation also have to be able to support the tundra vegetation, wetland soils, and peat development. Soils are mostly fine-grained or peaty, although other substrates do not necessarily preclude the development of polygonal structures.

I think the extensive re-use of figures and text from an earlier article in the study area section is too much.

→ Since the study site remains the same and in this case even the authors are the same, we do not see much necessity to re-invent this particular wheel for every publication coming from this site, especially since the relevant information will not change anyway.

You use values with 2 decimals throughout the paper. Is this the precision in you measurements? I would suggest using only values with 1 decimal in the paper.

→ Good point. We changed all values to one decimal.

You show in fig.2 the chamber setup is laid out south –southwest of the EC tower. However, the prevalent wind direction in the growing season of 2006 is from northwest and in less degree from east-southeast and south. Nested scales suggest concurrent and overlapping measurement (chamber within the footprint). With a prevalent wind direction from northwest this is not the case. How did you come up with the August footprint and what area did you use for the up- scaling? The method and steps used is not possible to follow at this stage.

→ We do not quite understand this comment. First, the chamber setup covers the entire sector from SE to SW of the tower. Second, we clearly stated the predominant wind direction in the manuscript, which was ESE, followed by S and WNW. Nowhere did we ever mention predominant wind directions from NW. Thus, in most cases, the chamber setup was upwind of the tower.

However, it does not even matter that much where in the footprint of the tower the chambers are, as long as they are in the footprint and as long as the classified image is representative of that footprint. The major differences in the fluxes are between the different classes / types of microsites, i.e. wet polygon center vs. moist/dry polygon rims or high centers and not between a wet polygon center north of the tower vs. one south of the tower. In addition, due to the unfortunate fact of not having simultaneous data from water bodies, there is no point in a daily comparison between chambers and eddy flux and we therefore decided to compare fluxes on a monthly basis. Obviously, for daily comparisons a detailed footprint analysis would have been necessary to know the exact area fraction and associated fluxes for each particular day. Over longer periods such as biweekly or monthly, however, we believe it is reasonable to assume that differences in footprint composition average out.

Page 3 Line 35 (1 ha- 1 km2) suggest to change ha to m2 (SI unit)

→ For consistency, we changed both units to m^2

Page 7 line 126 What do you mean about liquid precipitation, is snow in melted form included?
→ We only measured summer precipitation (rain=liquid) at the automated (non heated) tipping bucket rain gauge, so no snow is included. We changed the phrase “liquid precipitation” to “summer rainfall” to clarify.

Page7 line 132 What is the definition of growing season used?
→ The statement is based on our 10+ years of research on Samoylov Island and the typical start and end of vegetation growth. Using the thermal definition of the growing season beginning when temperatures are above 5°C for five consecutive days and ending when temperatures are below 5°C for five consecutive days would put the begin of the 2006 growing season at June 17th and the end at August 26th (due to a cold spell after which temperatures rose again).

Page 10 line 179 and Page 11 line 219 I would like to find out how much of the data was left after screening, Did you use measurements when rain and hard wind.
→ Measurements were not made when strong rain or snow storms had the potential to damage the analyzer. We changed “daily measurements” to “almost daily”. During the quality screening, ~ 11% of the measurements were discarded.

Page 16 line 321 is the StDev and SE the same? n=6?
→ This was indeed a case of *n=1* and therefore should not include a spatial standard deviation but just the standard error of the one measurements remaining after the quality screening.

Page 17 line 351 10…15, change to 10 to 15
→ Corrected.

Page 24 line 506-507. There are a difference in the fraction used in the ms and Schneider et al, how come?
→ The slight differences are due to Schneider et al. having used a different aerial image and a slightly different image section. We classified a newer image and only relied on Schneider et al. to separate overgrown water from very wet polygon centers, which they could differentiate during their supervised classification. Our unsupervised classification could not differentiate between these two classes, which look very much the same on the images and thus require expert knowledge to identify them manually. We corrected the references to clarify that.

Page 31 line 661 The reference is in Russian, or?, should be stated
→ Corrected.

Page 38 line 756- (Table 3) I assume you have averaged the 3 low center micro- sites into the class very wet soils and the flux value presented is the August average for all three micro-sites. Again, I think you should consider using values with only one decimal together with SE value. I do not understand the values (range) within brackets in Table 3.
→ That assumption is correct. We corrected the decimals and added an explanation of the values in the brackets: The class “open water” has a “background emission” via diffusion. Additionally, there may be occasional ebullition events that emit a lot more methane than the slow diffusive flux. The amount being emitted can vary strongly and the values in the brackets are the range for the ebullition flux.

Page 39 line 768 (Figure 2 text) You refer to Boike et al 2009 when presenting a mosaic of aerial images over Samoylov Island, however in Boike et al 2009, the images is only stated *very briefly and then the acquisition time is said to be 2006, not 2007. The Boike et al article is about climate, water- and energy balance and do not deal with remote sensing in anyway. I am interested in how the acquisition was made, platform (helicopter?), flight height, type of image etc. I do not find the reference Boike et al valid.*

→ We agree. The Boike et al. reference about climate, water- and energy balance is not the valid one – but it is also not the one referenced here. You are talking about Boike et al. 2008. We referenced Boike et al. 2009. While that is a mistake and should be Boike et al. 2008, it is not the JGR Boike et al. 2008 but an expedition report of 2008, which is now included in the reference list as Boike et al. 2008a. The acquisition information can be found in the same report on pages 5-7 by Scheritz et al.. Both balloons and helicopter were used for small-format aerial photography.

Page 39 line 788 (Figure 5 text). About surface temperature; you state surface temperature to be the only significant control of CH4. Is the surface temperature a measured parameter, in the ms text only soil temperature at different levels is mentioned, or as stated in the figure text a calculated temperature using Stefan-Bolzmann equation? If only calculated, this should be presented in the text, abstract etc

→ Surface temperature was calculated using the Stefan-Boltzmann equation. We included that information in the abstract and when at the first mentioning of surface temperature as a parameter relevant to the measured fluxes.

Page 45 (Figure 3). You state using 3 collars per micro site, however in figure 3, in the 4th image insert from the left, four collars are visible.

→ Actually, there are five collars visible in that image, but only three of those were used for measurements.

Page 48 Figure 7 P1-P5 is not explained; I would prefer R2 values and RMSE included on the graph. I find it interesting you use a linear regression, by using linear regressions you get a lot of high value outliers. How much would a non linear approach explain?

→ We included the R2 and RMSE in the graph. Non-linear approaches were tested during data analysis and found to explain less than the linear approach, which is why the latter was chosen.

Page 51 (Figure 9). I cannot find any references to this figure in the text, and I find it strange to use a classification and refer to an unpublished work.

→ References have been included in the text. This classification is indeed an otherwise unpublished classification that was made for this manuscript by a member of the working group who did not contribute to the manuscript except by producing the classification from aerial photography. That is a contribution to be acknowledged, but not one that warrants co-authorship.